This manuscript has been accepted for publication in *Geochemistry Geophysics Geosystems (AGU)* (https://doi:10.1029/2012GC004199). Please feel free to contact any of the authors; we welcome feedback.

Mukti, M. M., S. C. Singh, I. Deighton, N. D. Hananto, R. Moeremans, and H. Permana (2012), Structural evolution of backthrusting in the Mentawai Fault Zone, offshore Sumatran forearc, *Geochem. Geophys. Geosyst.*, *13*, Q12006,

Structural evolution of backthrusting in the Mentawai Fault Zone, offshore Sumatran forearc

M. Maruf Mukti & **Satish C. Singh**
L'équipe Géosciences Marines, Institut de Physique du Globe de Paris, CNRS, UMR 7154–Univ. Paris Diderot, Sorbonne Paris Cité, 1 rue Jussieu, FR-75238 Paris CEDEX 05, France
*(*E-mail: *mukti@tuta.io)*

Ian Deighton
TGS, Millbank House, 171-185 Ewell Road, Surbiton KT6 6AP, UK

Nugroho D. Hananto
Geoteknologi-LIPI, Komplek LIPI, Jalan Sangkuriang, Bandung 40135, Indonesia

R. Moeremans
L'équipe Géosciences Marines, Institut de Physique du Globe de Paris, CNRS, UMR 7154–Univ. Paris Diderot, Sorbonne Paris Cité, 1 rue Jussieu, FR-75238 Paris CEDEX 05, France

Haryadi Permana
Geoteknologi-LIPI, Komplek LIPI, Jalan Sangkuriang, Bandung 40135, Indonesia

[1] We present the interpretation of newly acquired high-quality industry-standard deep seismic reflection and swath bathymetry data to provide insight into the structural style and evolution of the Mentawai Fault Zone (MFZ). The MFZ lies along the boundary between the accretionary wedge and the proposed continental backstop. This zone exhibits arcuate ridges on the seafloor, convex toward the east. Beneath these ridges the structures developed as landward-vergent imbricated backthrusts in the inner part of the accretionary wedge and higher-angle backthrusts that deformed the forearc basin sediments. In the forearc high, anticlines were developed due to the seaward-vergent forearc high thrusts originating in the accretionary wedge. The imbricated backthrusts may have initiated during the Early-Middle Miocene contemporaneously with the slide and back-rotation of forearc high thrusts. In the Late Miocene, the higher-angle backthrusts were initiated. Continuous contraction induced the frontal higher-angle backthrusts and formed a fold-thrust belt toward the east during the Pliocene. The folds and thrusts were disturbed by diapirs and mud volcanoes. Backthrusting and fold-thrust belts developed in the MFZ may explain the compressional features observed at the boundary between the accretionary wedge and continental backstop along the southern Sumatra margin. The backthrusts along the MFZ are waning in activity and hence the risk of a large earthquake and associated tsunami at the present time should be small.

See more publications @ www.tektonesiana.org/publications

1. Introduction

[2] Present-day subduction along offshore Sumatra represents a classical example of oblique subduction, with a convergence rate varying from 60 mm/yr in the south to 52 mm/yr in northern Sumatra [*Prawirodirdjo and Bock*, 2004]. Deformation in such an oblique convergence setting is characterized by slip partitioning between the orthogonal and the arc parallel components, which are accommodated along the megathrust and Sumatra Fault, respectively [*McCaffrey et al.*, 2000]. It has been interpreted that slip partitioning of the arc parallel components was also accommodated by the Mentawai Fault (MF) and West Andaman Fault (WAF) [*Malod and Kemal*, 1996; *Mosher et al.*, 2008]. The MF has developed as a linear NW-SE trending feature along the western margin of the forearc basin from Nias Island to Sunda Strait [*Diament et al.*, 1992] (Figure 1).

[3] Uncertainties remain as to the origin of Mentawai Fault Zone (MFZ) [*Milsom*, 2005]. This zone was previously interpreted as a strike-slip fault system based on various features that resembled positive flower structures on the seismic profiles and its linearity on structure maps [*Diament et al.*, 1992; *Berglar et al.*, 2010; *Malod and Kemal*, 1996]. However, no strike-slip earthquakes were recorded in this region over the last 30 years [*Natawidjaja et al.*, 2006]. This fault zone was interpreted as overturned bedding cut by reverse faults [*Karig et al.*, 1979]. Furthermore, *Samuel and Harbury* [1996] suggested that the MFZ developed by inversion of originally extensional faults. Recent results based on shallow seismic reflection and bathymetry data suggest that the MFZ consists of a set of backthrusts in front of Siberut Island [*Singh et al.*, 2010]. Deep seismic reflection data have imaged a dipping reflector to 20 km depth that was interpreted to be a regionally extensive backthrust [*Singh et al.*, 2011]; this possible backthrust might be related to the MFZ. Moderate-earthquake clusters in 2005 and 2009 could involve displacement along this structure [*Wiseman et al.*, 2011]. A cluster of activity has been observed at the MFZ to the east of Pagai Island, with focal mechanisms of these events indicating thrusting [*Collings et al.*, 2012].

[4] Since the previous seismic data have limited resolution at depth, better subsurface imaging is crucial to reveal the complete structure and understand its kinematics. We had access to high-quality deep seismic reflection data along a significant portion of the MFZ [*Singh et al.*, 2009], 2D seismic data, and high-resolution swath bathymetry along a 900 km segment of the Mentawai forearc basin (Figure 1). We present images of the MFZ and interpret these for the structural style and distribution of the fault zone along the Mentawai Basin, and discuss the possible mechanism of major structures in the eastern margin of the accretionary wedge. The previous shallow seismic profiles were unable to image the complete structure in the MFZ. The new seismic reflection and swath bathymetry data provide evidence of compression structures developed within the accretionary wedge and forearc basin sediments.

2. Data and Methods

[5] In order to study the seismic and tsunami risks in the Mentawai locked zone [*Chlieh et al.*, 2008], a set of deep seismic reflection profiles were acquired by CGGVeritas. The CGGVeritas marine vessel Geowave Champion towed three streamers: One streamer was 15 km long towed at 22.5 m water depth, the longest streamer ever used, and two 6-km-long streamers were towed at 7.5 m and 15 m water depths. An array of air guns with a total volume of 9600 cubic inches, deployed at 15 m depth, was used as the seismic source [*Singh et al.*, 2009]. The shot spacing was 50 m and the record length was 20 s. The data were resampled to 4 ms and processed using 2–90 Hz anti-alias filter. An iterative velocity analysis was used in combination with 4–6 passes of radon multiple removal technique. The data from all three streamers were combined to obtain broadband seismic response [*Singh et al.*, 1996], and then processed using pre-stack Kirchhoff depth migration technique. The deep seismic profiles were about 260 km long but, here we only show the images around the forearc high and forearc basin. These lines were 220 km apart and hence allow mapping of only large-scale features.

[6] Independently, TGS had acquired seismic reflection data with a line spacing of 20 km. We

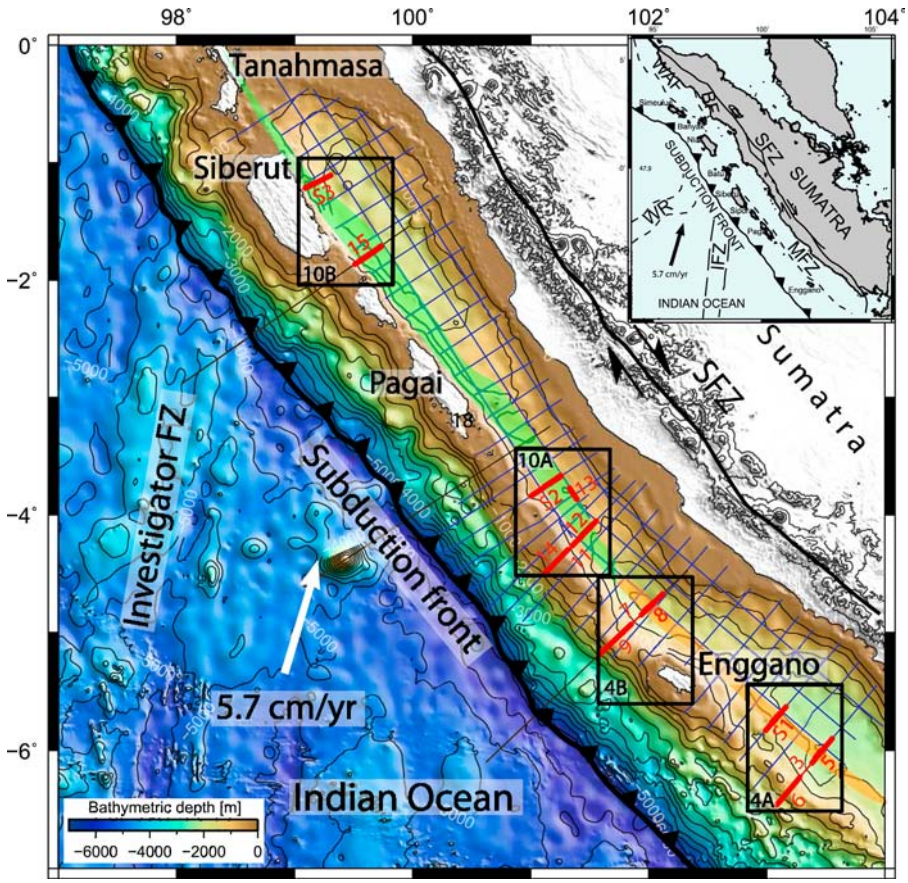

Figure 1. Shaded bathymetric map of Mentawai forearc. Blue and yellow lines indicate the location of all seismic profiles and red for the data shown in this paper. Black rectangles with numbers show blowup of features along MFZ (Figures 2 and 11). Shaded green and orange represents the MFZ. White arrow is the convergence vector after *Prawirodirdjo and Bock* [2004]. The regional bathymetry is from *British Oceanographic Data Centre* [2003], complemented by high-resolution swath bathymetry. Inset is the tectonic setting of Sumatra, MFZ = Mentawai Fault Zone, SFZ = Sumatra Fault Zone, BF = Batee Fault, WAF = West Andaman Fault, IFZ = Investigator Fracture Zone, WR = Wharton Ridge.

had access to 36 lines crossing the forearc basin along with 6 basin-parallel lines. These data were acquired using a 7.95 km-long streamer towed at 7 m depth and a 3940 cubic-inch air gun source towed at 5 m depth. The shot spacing was 37.5 m and the record length 12 s. The data were resampled to 4 ms and processed using a Kirchhoff pre-stack time migration technique.

[7] The surface expression of faults in the deformation zone was provided by the high-resolution swath bathymetric data and the global bathymetry of GEBCO [*British Oceanographic Data Centre*, 2003]. The high-resolution swath bathymetric data in this area is a compilation of German data set [*Ladage et al.*, 2006] recorded during the SeaCause cruises. The data sets were ping edited and provided as grid data in xyz-ASCII format. Gridding was performed with a grid spacing of 100 m and plotted in maps with the Generic Mapping Tool (GMT) software [*Wessel and Smith*, 1991].

[8] The seismic reflection and bathymetry data were interpreted along with accurately relocated earthquakes using the double-difference method [*Pesicek et al.*, 2010] to determine the location of active faults. The focal mechanisms from GCMT catalog (1976–2010) helped us constrain the geometry of the structures.

[9] The structural interpretation of seismic reflection data is constrained by the growth strata, which, where imaged, record the time of development of the structures. Deformation of the folds and thrusts is investigated by analyzing the growth strata architecture preserved on the structure fold limbs [e.g., *Poblet et al.*, 1997]. The stratigraphic intervals are divided into seismic units that are bounded by major seismically defined stratigraphic surfaces,

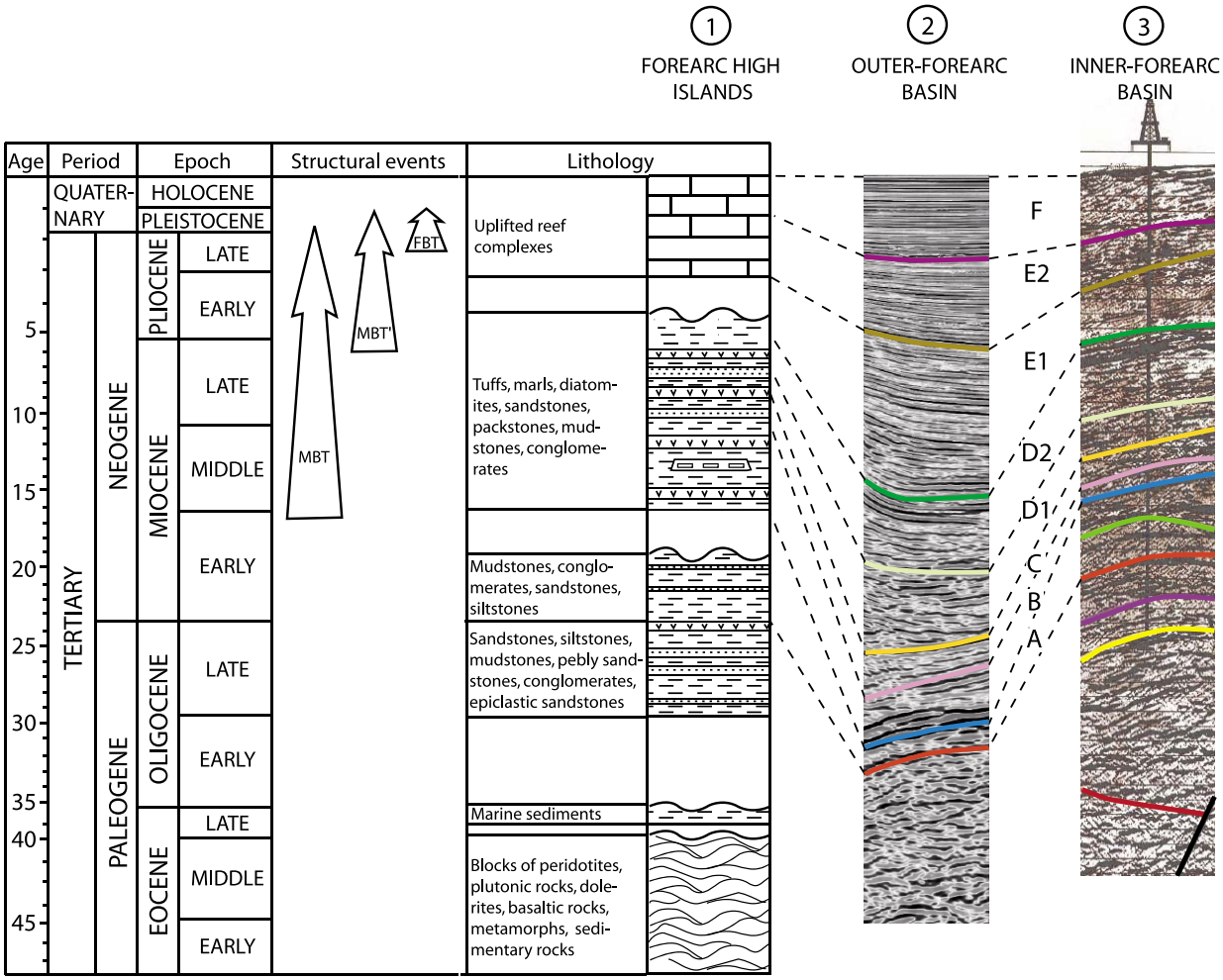

Figure 2. Correlation of well and outcrop data from study area and their megasequences: 1 = Stratigraphic column of Nias Island and part of Siberut after *Samuel et al.* [1997]; 2 = seismic line in this study; 3 = seismic line in the inner forearc basin after *Hall et al.* [1993]. Structural events are interpreted from this study.

which often correlate with important geological events. The horizons at the top of seismic units are picked as chrono-stratigraphically significant surfaces based on onlap relationships, truncated reflections, and contrasts between seismic facies reflectivity.

[10] The seismic horizons can be correlated to the top of megasequences interpreted from a seismic line in the shallow part of forearc basin, which includes the area from the present shelf landward. Age dating of the megasequences were constrained by the Arwana-1 well data [*Hall et al.*, 1993], which is located ~0.7 km to the north of the northeast tip of one of the profile. The Arwana-1 exploration well, which was drilled to a total depth of 4,175 m, reached the upper part of the oldest megasequence. The seismic units have been divided into 4 mega-sequences constrained by biostratigraphic analyses of the well data [*Hall et al.*, 1993]. The megasequences show a relatively complete Cenozoic section from the Early Oligocene or possibly Late Eocene.

[11] In the deeper part of the present forearc basin, the basin fill can be divided into 6 units that can be correlated to the megasequences determined in the shallow part (Figure 2). Unit A represents the Lower Miocene sediments (Figure 3). There are several horizons beneath Unit A that can be correlated with the Upper Eocene to Lower Miocene sediments in the inner forearc basin (Figure 2) [*Hall et al.*, 1993]. Unit A correlates with a package of high-amplitude, low-frequency reflectors with a progradational pat-tern dipping toward the west. At depth, the reflectors become less clear. This unit may correlated with the upper part of the Middle Oligocene-Lower Miocene Oyo and Gawo Formations in Nias Island [*Samuel et al.*, 1997]. The base of these sediments is not mappable beneath the top of the accretionary

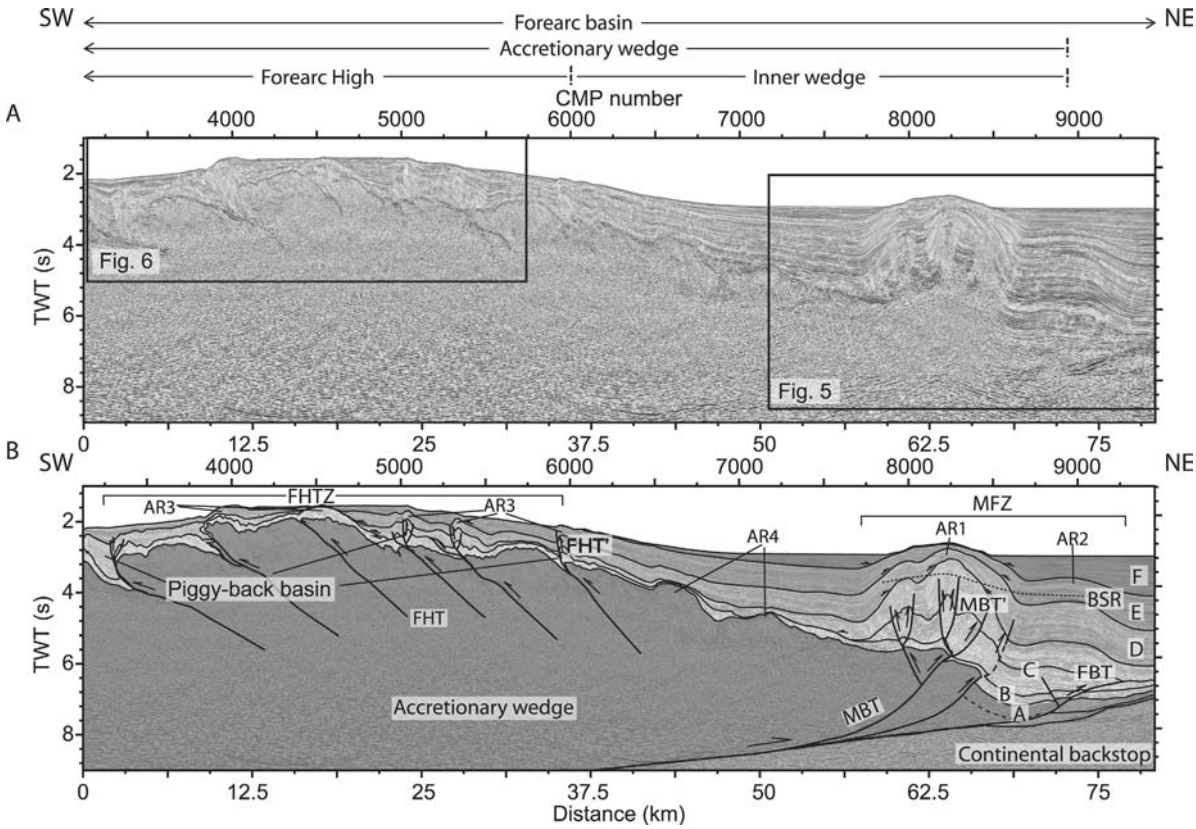

Figure 3. (a) Uninterpreted seismic section and (b) interpreted seismic section of line SSS-135 showing the structures in the MFZ and forearc high: AR = anticlinal ridge; MBT = imbricated backthrust; MBT′ = higher-angle backthrust; FBT = frontal higher-angle backthrust; FHT = forearc high thrust; BSR = Bottom Simulating Reflectors. Units A – F represent megasequences of the Middle Miocene-Recent forearc basin sediments. Small black arrows indicate termination of reflectors.

wedge. The exposures of Gawo Formation in Nias show intense deformation compared to the overlying sediments [*Samuel et al.*, 1997]. Such deformation could be the cause of the chaotic seismic facies character beneath the top of the accretionary wedge (Figure 3). Within the MFZ, the top of Unit A seems to correlate with the top of a chaotic to non-reflective zone, possibly indicating intense deformation (Figure 3). This horizon can be traced farther west, and was interpreted as the top of the accretionary wedge [*Schlüter et al.*, 2002; *Susilohadi et al.*, 2005]. However, it is not possible to map the base of Unit A and the horizons of older sediments beneath the accretionary wedge.

[12] Unit B corresponds to Middle Miocene sediments, and to the west this unit shows thinning to the top of accretionary wedge. Units C and D are Upper Miocene sediments, and these units show thinning to the forearc high. Units E and F represent Lower Pliocene-Recent sediments. Units B to F were deposited overlying the accretionary wedge sediments, and are here referred to as the Middle Miocene-Recent forearc basin sediments (Figure 3).

[13] The landward portion of the accretionary wedge is characterized by landward dipping wedge (Figure 3, CMP 6000–8800), here referred to as the inner wedge of *Wang and Hu* [2006] (Figure 3). To the west, the accretionary wedge is characterized by development of seaward-vergent imbricated-thrusts (Figure 3, CMP 3100–6000), here referred to as the forearc high. The outer wedge, or the seaward portion of the accretionary wedge, which dips toward the southwest is not discussed here.

3. Deformation in the Forearc

[14] Based on structures on the seafloor along the MFZ and their relationship with the deeper structures, the study area can be divided into two segments; (1) the Enggano Segment, where the MFZ is aligned along an azimuth of 309° from the north of Enggano Island (4.5°S) to near the Sunda strait

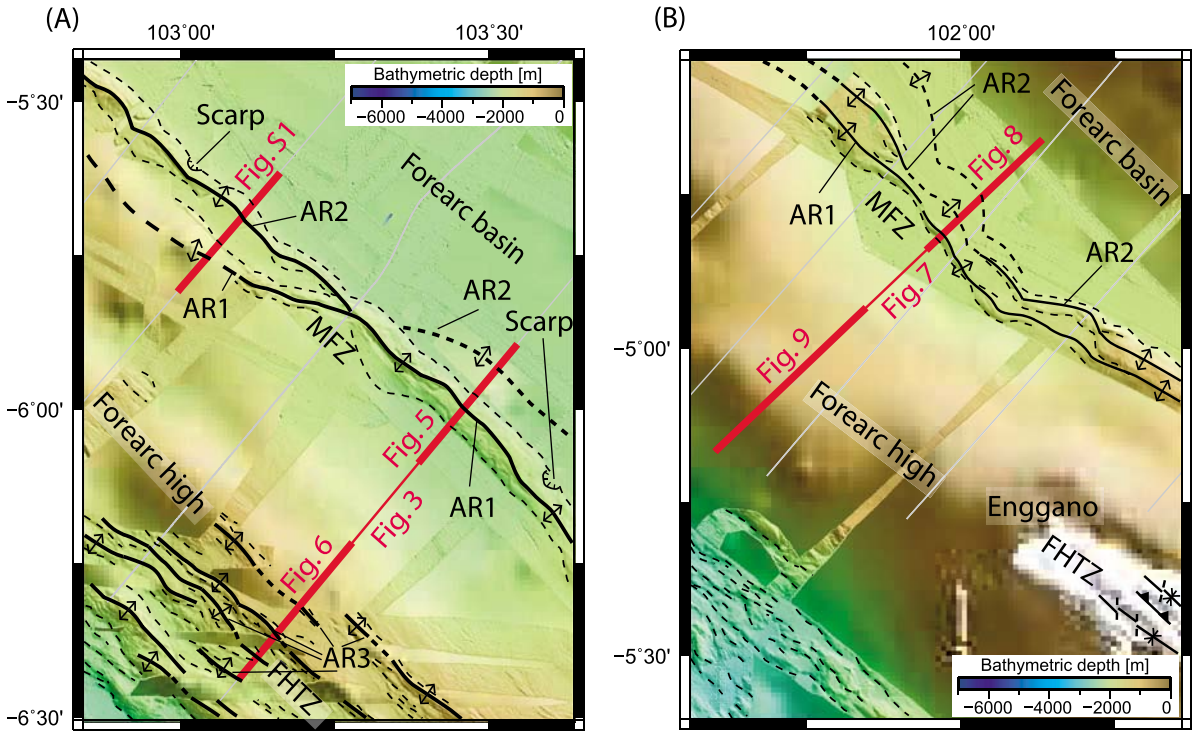

Figure 4. Bathymetric features of MFZ along the Enggano Segment in the (a) southeastern and (b) northwestern part. AR = anticlinal ridge. FHT = forearc high thrust. Solid thick black line is the axis of the anticlines. Dashed tick line marks the extent of anticline observed on the seismic profiles. Dashed thin black line represents the limb of the anticlinal ridges. Thin highlighted gray lines represent the seismic lines, and red lines for the data shown in this paper. Note slide escarpment on the NW limb of the ridge. Solid thick blue line is the axis of anticlines in the forearc high. Dashed thin blue line represents the limb of the anticlines. Fold and seaward-vergent thrust developed in the Enggano Island.

(7.5°S), and (2) the Siberut-Pagai Segment, where the MFZ trends at an azimuth of 321°, from north of Siberut (0.5°S) to north of Enggano Island (Figure 1). In the Siberut-Pagai Segment, the MFZ develops along the eastern margin of the forearc high. The fault zone starts to bend ∼11° counterclockwise in the northern Enggano Segment (4.5°S) and turns toward the basin in the southeast. In both regions, the MFZ mimics the trend of the subduction front and alignment of the present forearc basins, although the distance between the MFZ and subduction front is different in the two segments. The distance between the subduction front and the MFZ increases from 120 km in the north to 170 km in the south.

3.1. Enggano Segment

[15] In the Enggano Segment, positive features on the seafloor are aligned in a NW-SE trend for 340 km (Figure 1). These are arcuate-shape ridges that are convex toward the NE (Figure 4). There are at least two ridges observed on the seafloor and in the subsurface, which here defined as Anticlinal Ridges 1 (AR1) and Anticlinal Ridge 2 (AR2) (Figure 3). The former structure has a wider area than the latter: AR1 has a ∼200 m high relief and is ∼9 km wide, and to the east, AR2 is ∼150 m high and ∼4.5 km wide. AR1 is continuous along the NW trending alignment, developed in the center of the basin in the south of Enggano and close to the forearc high in the southeast of Pagai (Figures 1 and 4). AR2 formed as discontinuous ridges, and locally some of these ridges are covered by young sediments (Figure 4b). Spacing between these ridges is up to 8 km. A single ridge on the surface can reach 100 km in length. A 4.6-km wide headwall scarp can be observed on the NE limb of AR 1 (Figure 4a, 6°7′ S). This escarpment is concave toward NE, which may indicate the direction of the sliding.

[16] Beneath these ridges, folding and faulting are interpreted to have deformed the thick (4 s TWT) forearc basin sediments (Figure 3). Offset sedimentary reflectors can be observed beneath AR1. These structures can be interpreted as a set of high-angle thrusts that deformed the sediments of units B to D (Figures 3 and 5). Reflectors of the upper part

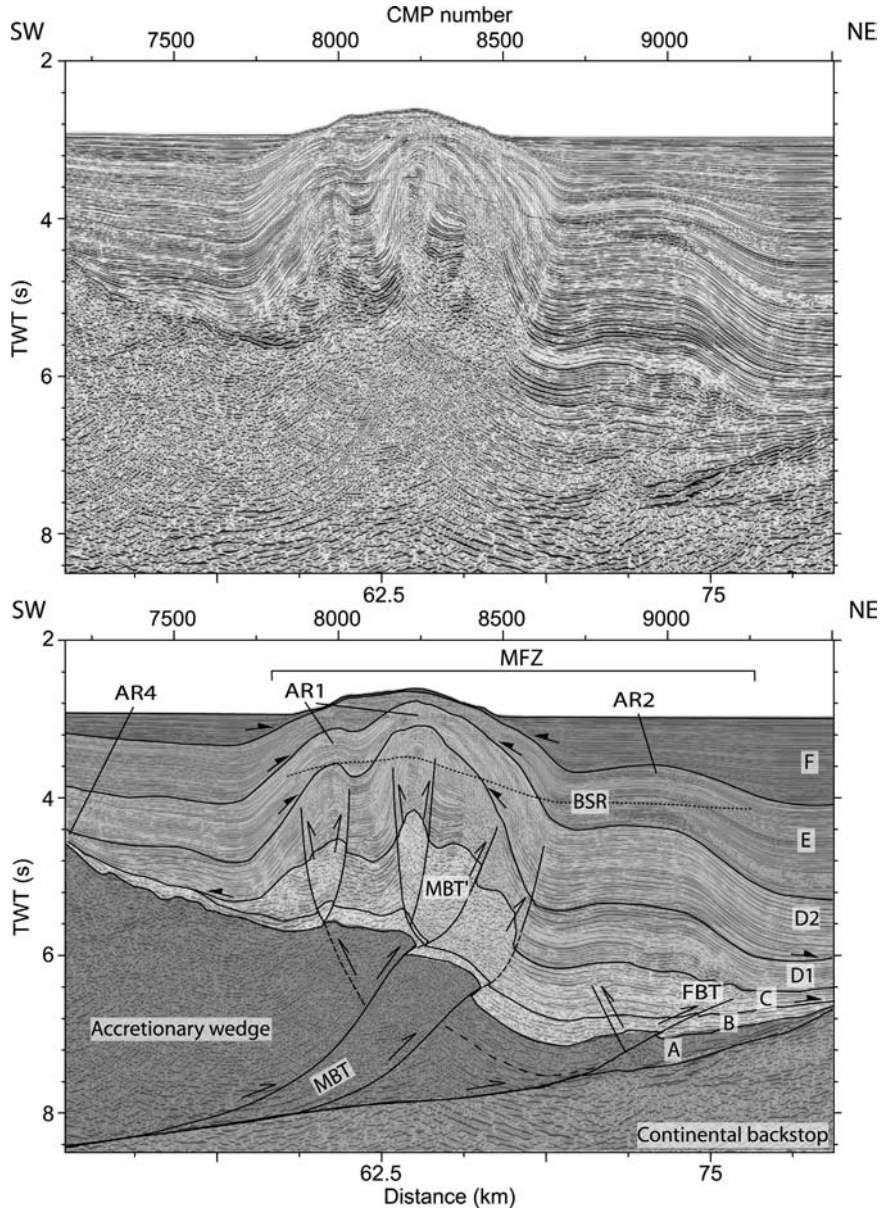

Figure 5. (top) Uninterpreted seismic section and (bottom) interpreted seismic section of line SSS-135 across the MFZ. See caption in Figure 3 for the abbreviations.

of Unit D or Unit D2 show onlap to the limbs of anticline formed by the lower part of D, or Unit D1. The growth of Units E and F shows thinning to the forearc high and to the limbs of the anticline. Unit F is flat and diverges toward the anticline.

[17] Dipping reflectors are observed beneath the top of the inner wedge. We interpreted these to be imbricated backthrusts that have deformed sediments up to Unit A (Figures 3 and 5). Beneath AR2, a set of thrusts have folded sediments up to Unit E. Onlap reflectors of Unit F can be observed to the top of Unit E. Unit B shows thinning to the forearc high. These thrusts appear to continue at depth into a horizon of high amplitude reflectors that are interpreted as a fault surface dipping to the west.

[18] To the west of the MFZ, a zone of NW trending elevated features can be observed on the seafloor along a ~40 km wide forearc high (Figure 4a). Seismic profiles show the features that are here referred to Anticlinal Ridge 3 (AR3), which involve ~1.3 s TWT thick sediments (Figure 6). These anticlines have formed above thrusts that can be differentiated into two types, (1) the thrusts that deformed the forearc basin sediments deposited in

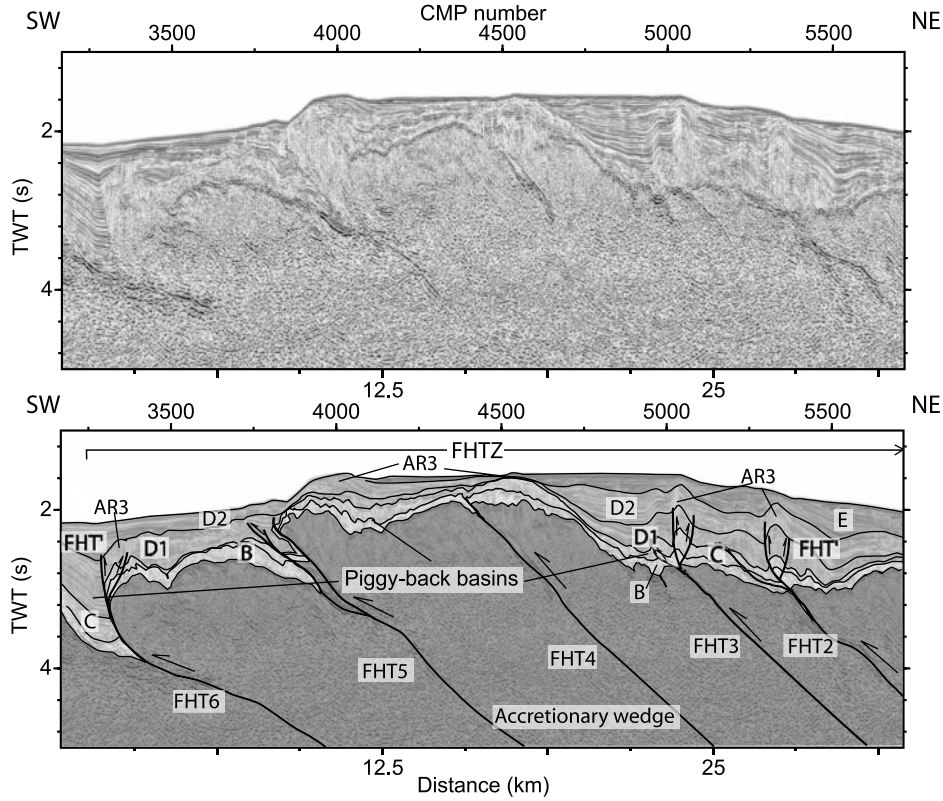

Figure 6. (top) Uninterpreted seismic section and (bottom) interpreted seismic section of line SSS-135 across the forearc high. FHT = forearc high thrust; FHT′ = higher-angle forearc high thrust.

the piggyback depressions, and (2) the seaward-vergent imbricated thrusts that can be observed beneath the top of the accretionary wedge (Figure 6). The thrusts that developed in the piggyback depressions have folded sediments up to Unit C. Onlap of reflectors of Unit D to the folded Unit C can be observed. Unit D shows thicker sediments in the area between the anticlines and thinning to the margin of the piggyback depression. The seaward-vergent imbricated-thrusts can be observed cut through the accretionary wedge sediments from the depocenter of the piggyback depressions down to ~5 s TWTT. Unit B is thicker in the depocenter of the piggyback depression, and shows thinning to the margin of the depression.

[19] Structural highs can be observed in the inner wedge, between the MFZ and the forearc high (Figure 3). These structures formed by folding of the sediments of the accretionary wedge, here referred to as Anticlinal Ridge 4 (AR4). Unit B shows thinning onto the anticlines, indicating that the structures may have developed prior to deposition of Unit B (Figure 5). There is no offset of reflectors beneath the top of the accretionary wedge, indicating that these structures might have formed as buckle folding due to compression. Another possibility is that these structures could simply reflect the mechanical properties of weak materials surrounding the structure with little overburden.

[20] To the northwest, we interpret AR1 as the surface expression of thrusts that can be observed in the overlying thick forearc basin sediments up to Unit D (Figure S1 in the auxiliary material).[1] Units D-E show thinning onto the limbs of this anticline. The top of Unit F is flat, but shows higher elevation in the area to the west of the anticline compared to the area in the east. Reflectors of Unit F show onlap termination to the limbs of the anticline. Dipping reflectors can be observed beneath the top of the accretionary wedge. We interpret these features as landward-vergent imbricated thrusts. These structures show a similar pattern with those in the SE. Normal faults have developed on top of AR1 that deformed the forearc sediments up to Unit D. Chaotic reflectors seem to dominate the core of the anticline.

[21] Folded sediments up to Unit E can be observed to the east of AR1 (Figure S1). The pattern of these

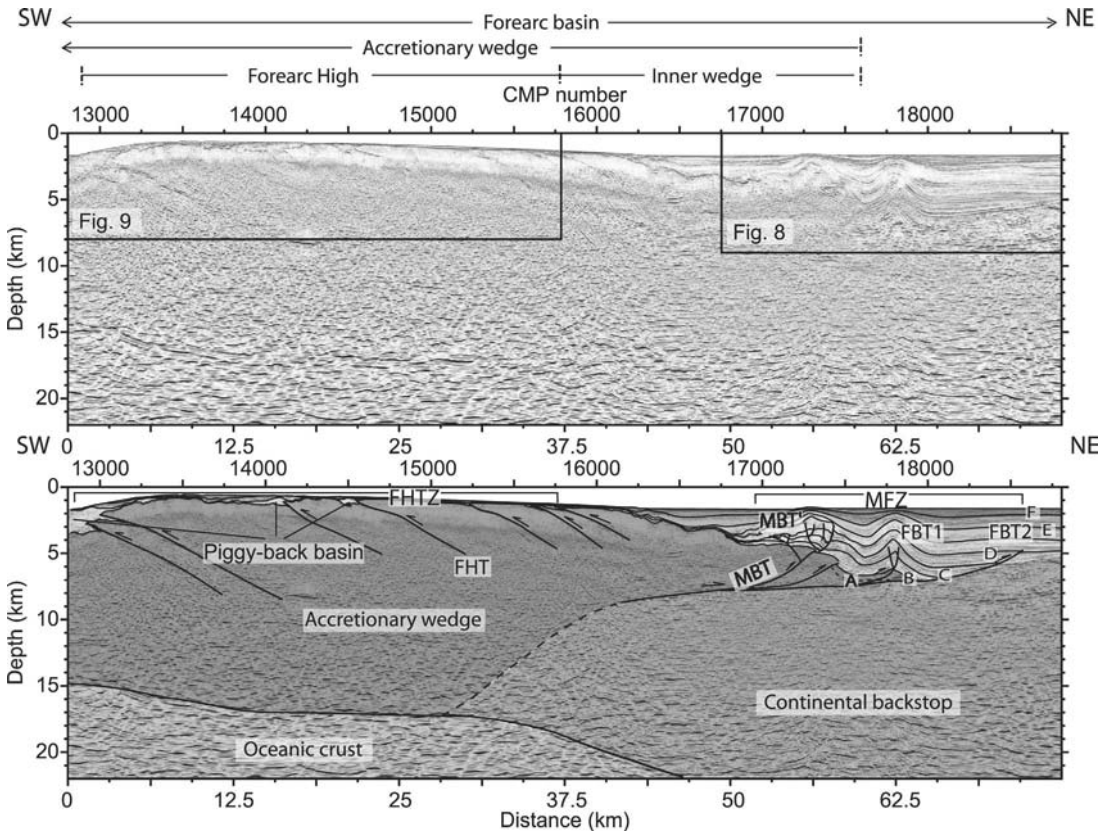

Figure 7. (top) Uninterpreted seismic section and (bottom) interpreted seismic section of line CGGV040 showing structures in the MFZ and forearc high. Note the deeper extent of MBT to the top of oceanic crust along the continental backstop.

sedimentary units indicates that this anticline (AR2) formed after the formation of AR1. Unit F shows thinning to the limbs of the anticline. Beneath the anticline, a landward-vergent thrust has developed and seems to continue to the landward-vergent imbricated thrusts beneath the accretionary wedge. A headwall scarp (2.5 km wide) has formed on the NE limb of AR2 (5°36′S), suggesting mass-wasting on the slope of ridge (Figure 4a).

[22] To the north of Enggano Island, a pre-stack depth migrated image of CGGV040 shows a similar seismic character of structures to those developed in the south (Figure 7). The forearc basin sediments deposited on the slope to basin in the southeast side and accretionary wedge to southwest. In the MFZ, AR1 is 6 km wide but is asymmetric, and exhibits complex small-scale folding bounded by thrusting dipping at 40–50° (Figure 8). These thrusts deformed the forearc basin sediments up to Unit D. The growth of Unit E shows thinning to the top of accretionary wedge and to the limbs of AR1. The top of Unit F is flat, and this unit shows thinning toward the limbs of anticline. Dipping reflectors are observed beneath the top of the accretionary wedge that dip 30–35° (Figure 8); we interpret these as imbricated backthrusts. Packages of reflectors within Unit B show thinning in the area of these thrusts. Beneath the forearc high, the dipping reflectors that are interpreted as backthrusts seem to continue at depth along a reflective surface. We interpret this reflective surface as a higher-angle fault that terminates at the top of the subducting oceanic crust (Figure 7).

[23] To the east, folded reflectors within Unit E1 and older sediments are observed and formed anticline (Figure 8). Units of E2 and F show thinning toward AR2. Beneath the structures, seaward dipping reflectors (∼70° and ∼25°) are observed. We interpret these reflectors as landward-vergent thrusts that seem to have developed and rooted on to the imbricated thrusts beneath the inner wedge. In the area between CMP 18400–18600, displacements of Unit C and D1 are observed over a fault ramp of about 250–130 m wide (Figure 8). These landward-vergent thrusts are interpreted to have merged in to the gentle dipping (∼5°) fault and seems rooted at depth on to the imbricated thrusts.

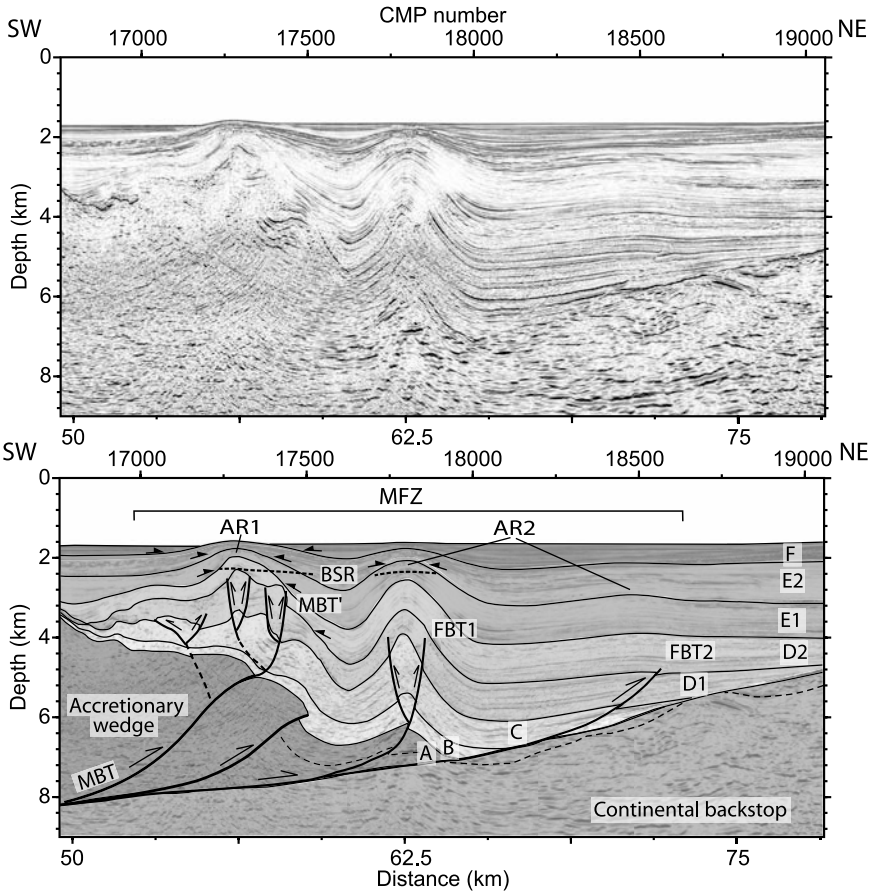

Figure 8. (top) Uninterpreted seismic section and (bottom) interpreted seismic section of line CGV040 across the MFZ. Unit F is flat, show thinning to AR1. Reflectors of Units D and E show onlap to the anticline.

[24] To the west of the MFZ, multiple low angle thrusts (23–30°) can also be observed beneath the eroded forearc high to the north of Enggano Island (Figure 9), similar to those observed in the south of Enggano. The forearc high seems to have been tilted toward the NE, as indicated by the dip of the flat younger sediments deposited over the unconformity. Based on their stratigraphic position, these flat sediments can be correlated with the Pleistocene limestones exposed in Enggano Island [*Amin et al.*, 1993].

3.2. Siberut-Pagai Segment

[25] In the 600-km-long Siberut-Pagai Segment, AR1 reaches 500 m high and is up to 8 km wide. AR2 is ~250 m high and ~4.5 km wide. The spacing between these ridges is up to 13 km (Figure 10). Each of these ridges exhibits an arcuate shape that is convex toward the east and up to 20 km long. Dipping reflectors can be observed beneath AR1. We interpret these reflectors as backthrusts that have deformed the forearc basin sediments (Figure 11). The backthrusts have folded sediments up to Unit D (Figure 12). A truncation surface can be recognized within Unit E and continues toward the forearc high (Figures 12 and S2). Units E and F shows thinning to the forearc high and around the limbs of anticline (Figure 11). To the east, anticlines have formed by folding sediments up to Unit E (Figures 12 and S2). The top of Unit F is flat and the reflectors show onlap to the limbs of anticlines. Dipping reflector can be found beneath AR2 and we interpret this as a higher-angle backthrust.

[26] Anticlines can be observed to the west of AR1 (Figures 12 and S2). Offset sedimentary reflectors can be recognized within these anticlines. We interpret these structures as higher angle thrusts. There is a subhorizontal reflector above the top of the accretionary wedge, whereas there is no obvious offset of sedimentary reflectors beneath the accretionary wedge. We suggest that these higher angle thrusts have developed within a detachment surface along the top of the accretionary wedge.

[27] A conical feature on the seafloor can be recognized within the fold-thrust belt with a 1.5-km-

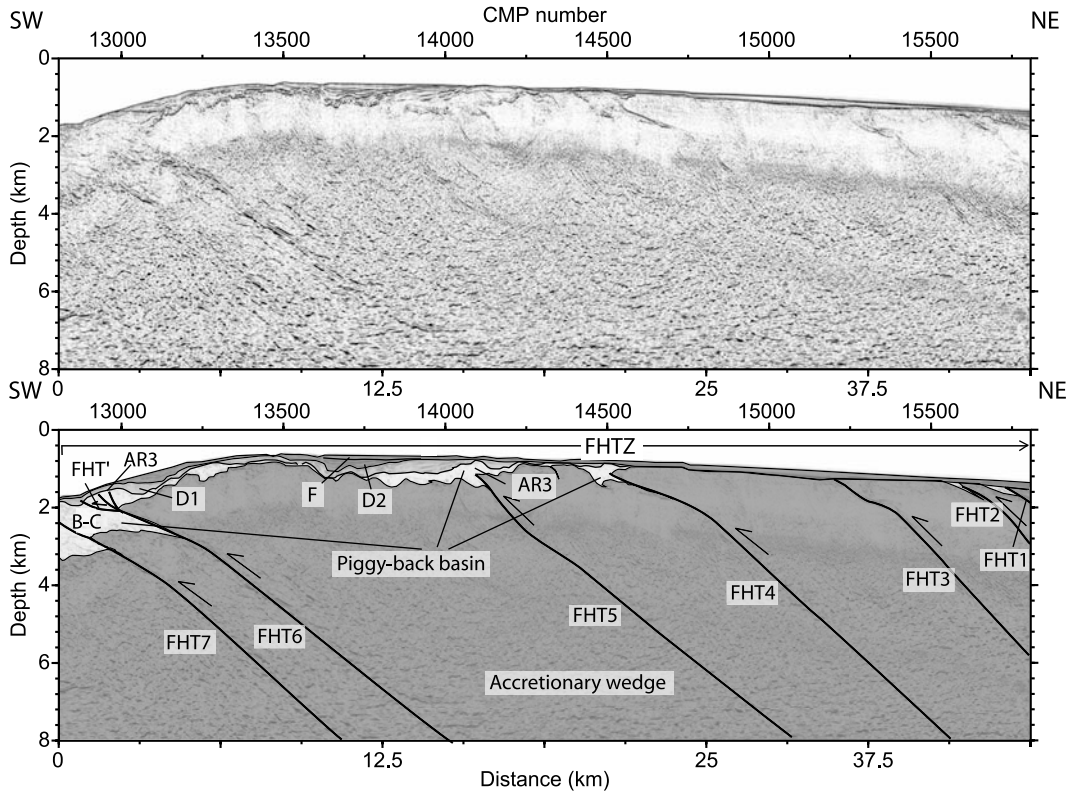

Figure 9. (top) Uninterpreted seismic section and (bottom) interpreted seismic section of line CGGV040 across the forearc high. Note truncation of accretionary wedge and forearc basin sediments.

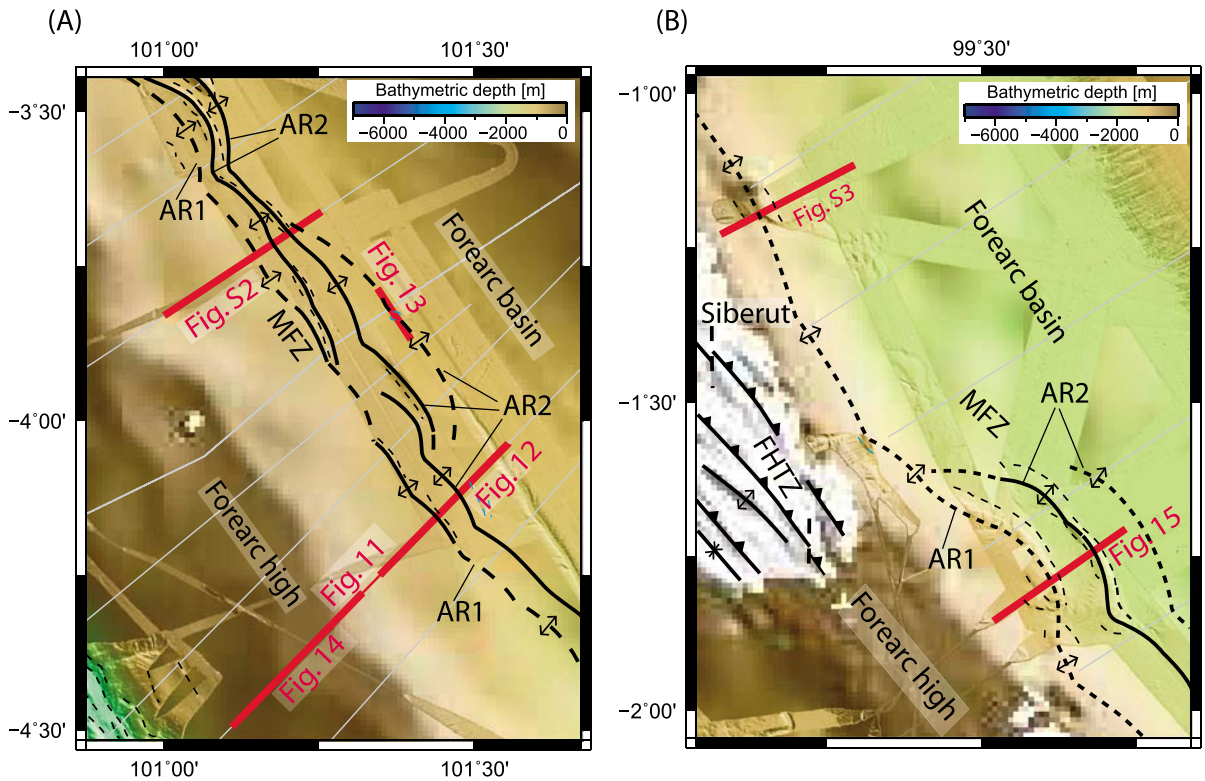

Figure 10. Bathymetric features of MFZ in the (a) southeastern part and (b) northwestern part of the Siberut-Pagai Segment. Red lines are the seismic profiles shown in this paper. Folds and thrusts developed in Siberut Island.

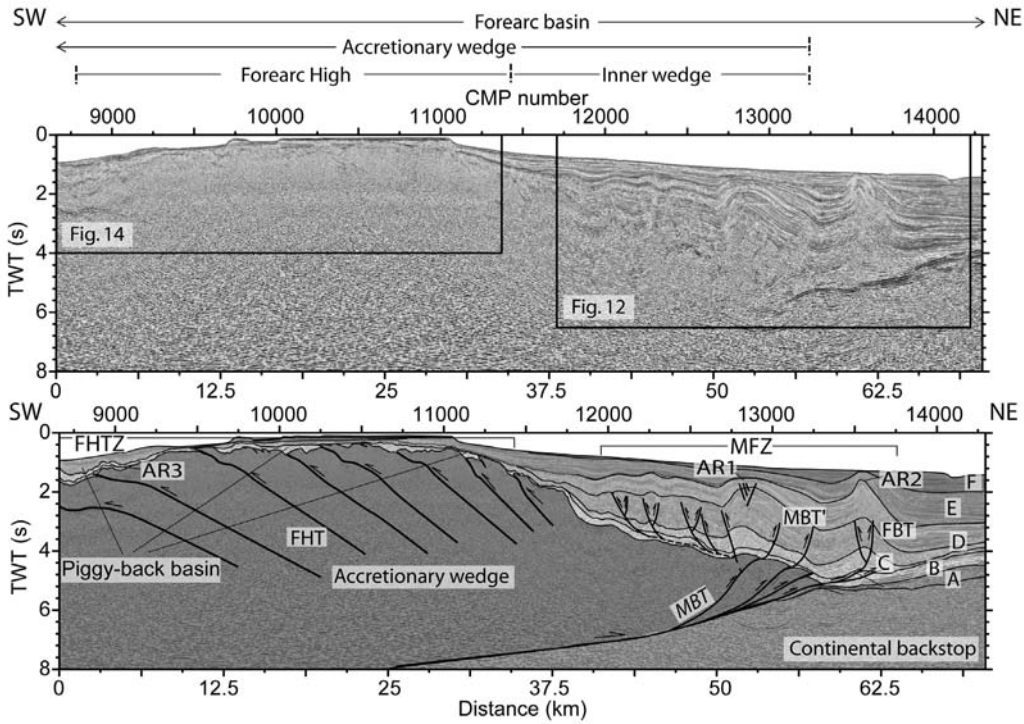

Figure 11. (top) Uninterpreted seismic section and (bottom) interpreted seismic section of line SMI-223 showing the MFZ and forearc high. Sediments on top of the forearc high were eroded. Dashed line marks the unconformity in the forearc basin.

diameter (Figure 10a). The seismic profile across the eastern limb of this feature shows that normal faults have deformed the sedimentary reflectors down to Unit E (Figure 13). Furthermore, the reflectors of Units C to E are convex upward with internal chaotic reflectors. These observations may indicate a diapiric process, where injected materials from a deeper part penetrated the younger sediments.

[28] Seaward dipping reflectors can be observed beneath the inner wedge, and can be interpreted as imbricated landward-vergent backthrusts (Figure 12), resembling those in the Enggano Segment. Parallel bedded facies can be recognized beneath the top of the accretionary wedge in the fold-thrust belt, indicating the continuity of sediments up to Unit A in the accretionary wedge to the west. Unit B was deposited overlying the accretionary wedge and shows thinning toward the imbricated backthrusts. The continuity of the folds and thrusts belt to the west cannot be constrained due to the poor resolution of the seismic image at depth.

[29] Folded sediments can be recognized in the forearc high that formed AR3 (Figure 14). Beneath these anticlines, dipping reflectors can be observed. We interpret these reflectors to be seaward-vergent imbricated thrusts resembling those in the Enggano Segment. These structures are represented by eight closely spaced (4–11 km) seaward-vergent thrusts. A truncation surface can be found within the accretionary wedge and forearc basin sediments (Figures 12 and 14).

[30] The anticlines on the seafloor become difficult to trace farther north due to the limit of our swath bathymetry coverage (Figure 10b). However, AR1 can still be observed on the seismic profiles that indicate its continuation to the north. On the pre-stack depth migrated image of CGGV010, offset sedimentary reflectors can be observed beneath the anticlinal ridges. We interpret these features as higher angle backthrusts that have deformed ~5.5-km-thick forearc basin sediments (Figure 15). These faults dip at 40–50°. AR1 has folded sediments up to Unit D, as indicated by onlap of reflectors of Unit E to the limbs of the anticline. AR2 has folded sediments up to Unit E, indicated by onlap reflectors of Unit F to the limbs of the anticline. The forearc basin sediments show thinning to the forearc high. Offset sedimentary reflectors can be recognized beneath the inner wedge. We interpret these features as imbricated backthrusts (Figure 15). These backthrusts dip at 32–38°, show lower dip compared to the higher-angle thrusts. The inner wedge developed in the hanging

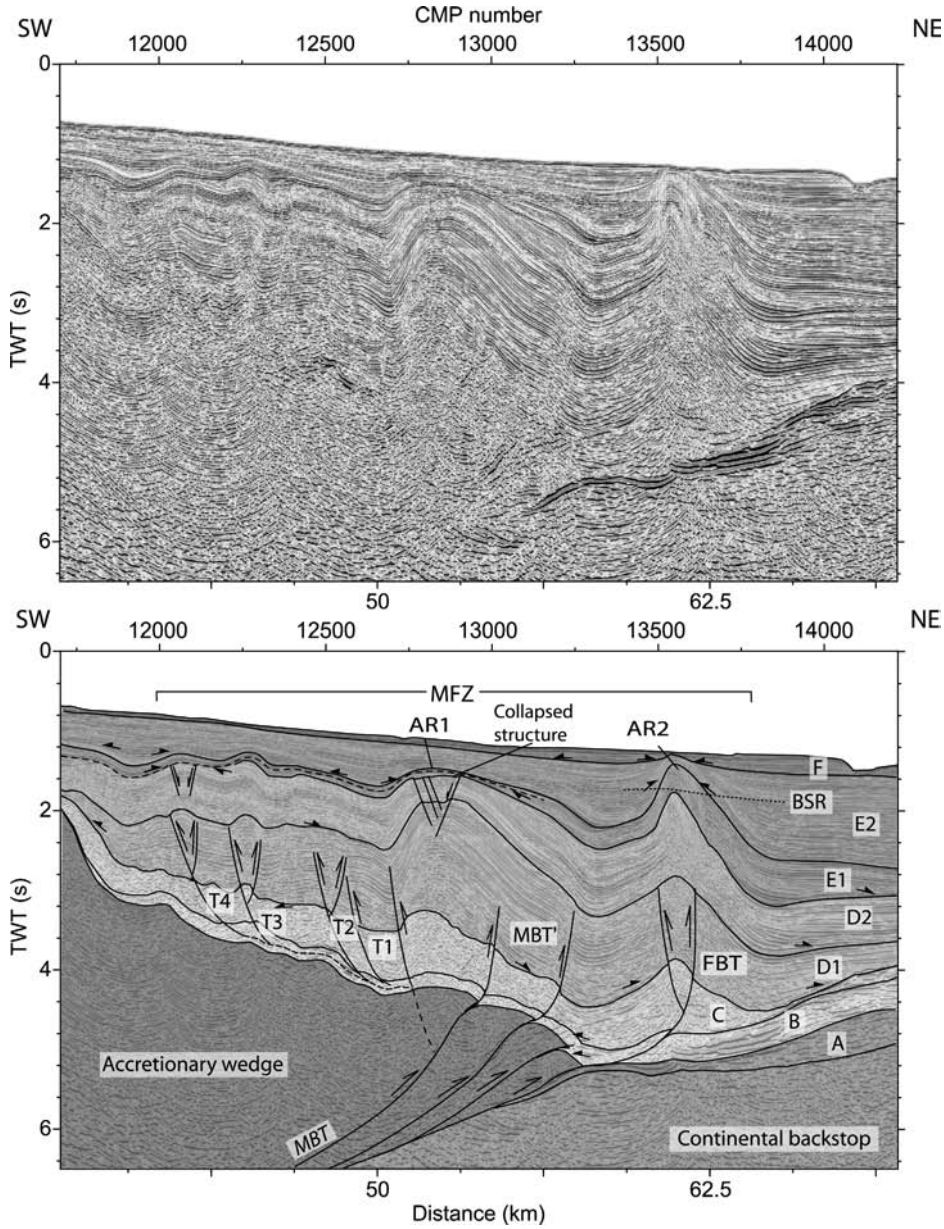

Figure 12. (top) Uninterpreted seismic section and (bottom) interpreted seismic section of line SMI-223 across the MFZ. Note collapsed structure on AR1. Dashed line marks the unconformity in the forearc basin.

wall along a gentle dipping (4°) detachment surface and formed a ~19° taper angle, which is steeper than that in the Enggano Segment.

[31] Farther north, it is difficult to infer the exact position of the backthrusts due to limit of the seismic lines coverage. However, anticlinal ridges can be observed to the east of Siberut Island, indicating continuation of the anticlines (Figure S3). AR1 has folded sediments up to Unit D, as indicated by onlap of reflectors of Unit E to the limbs of the anticline. To the east of this anticline, sediments up to Unit E are slightly folded that formed AR2. The reflectors of Unit F onlap the limbs of the anticline. These observations indicate the possible continuation of the thrusts. To the west of AR1, a structural high has formed by folding of the accretionary wedge sediments here referred to as AR4 (Figure 15). Units B-E show thinning toward this anticline.

4. Interpretation of Structural Analysis

[32] Based on our interpretations, the deformation zone in the southern Sumatran forearc can be divided

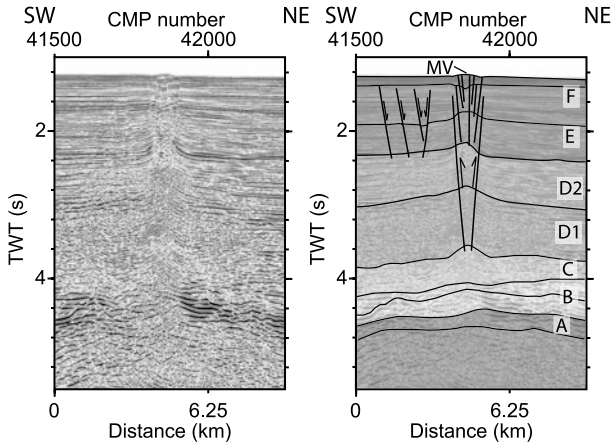

Figure 13. (left) Uninterpreted seismic section and (right) interpreted seismic section of a strike line SMI-200 crossing a mud volcano (MV) developed in the MFZ. Conical structure exhibits in the seafloor. Collapsed structure bounded by vertical faults as a conduit for releasing material at depth to the seafloor.

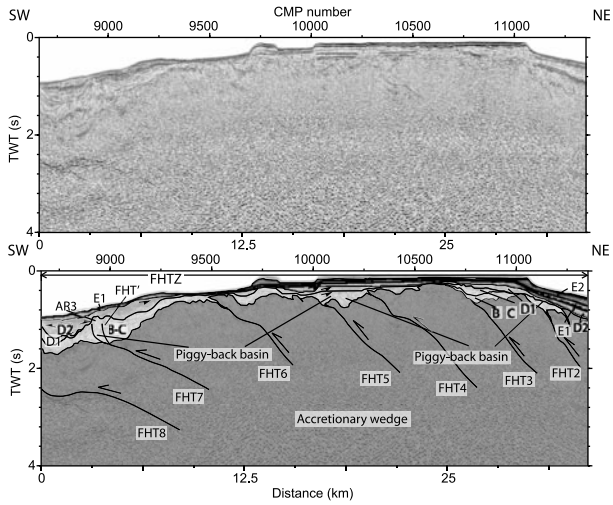

Figure 14. (top) Uninterpreted seismic section and (bottom) interpreted seismic section of line SMI-223 across the forearc high. Note truncation of the forearc basin sediments.

into the MFZ that is dominated by landward-vergent backthrusts and the forearc high thrust zone (FHTZ) that formed by seaward-vergent thrusting (Figures 3 and 11). In the Mentawai forearc, the surface expression of the MFZ can be observed as NW-trending arcuate ridges on the seafloor. Beneath these ridges, folds and thrusts have deformed the forearc basin sediments. The elements of the fault system will be described below. Based on the observation of growth strata, different ages can be assigned to these fault elements.

4.1. Backthrusting in the MFZ

[33] The imbricated backthrusts can be referred to as multiple components of the Main Backthrust (MBT) of *Singh et al.* [2010], which previously has been interpreted as a single structure (Figure 3). These imbricated backthrusts formed a structural high in the inner wedge, and involved sediments up to Unit A. Unit B shows thinning to the tip of these backthrusts. To the south of Pagai, Unit B shows thinning in the area beneath AR1, and is slightly thicker westward (Figure 12). Based on the geometry of the growth strata and onlap termination of reflectors of Unit B to the overlying Unit A, the imbricated backthrusts may have developed prior to deposition of Unit B, or during the Early-Middle Miocene. We suggest that the imbricated backthrusts were waning during the Middle-Late Miocene, as indicated by constant thickness of Units C and D and the parallel relationship between reflectors of those units (Figure 12).

[34] Beneath AR1, backthrusting has folded sediments up to Unit D. Reflectors of Unit D2 show onlap to the limbs of AR1 (Figure 5). These observations indicate that these higher-angle backthrusts, developed after deposition of Unit D1 and before deposition of Unit D2, or during the Late Miocene.

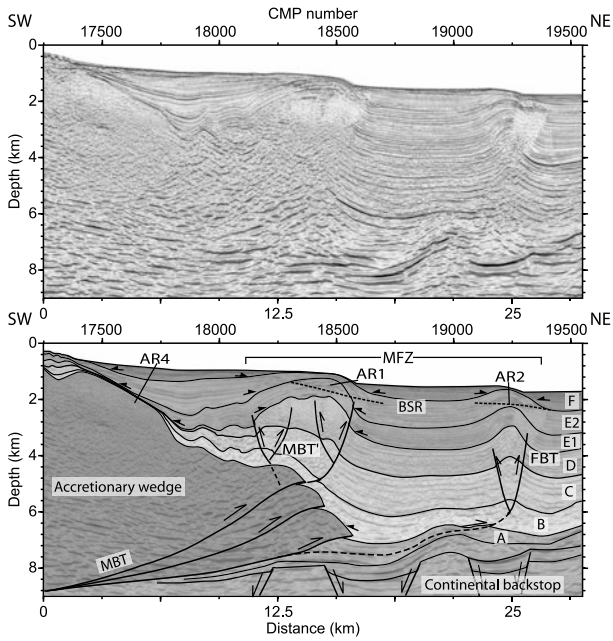

Figure 15. (top) Uninterpreted seismic section and (bottom) interpreted seismic section of line CGGV010 across the MFZ. Normal faults formed the horst and graben structure in the Paleogene sediments.

Onlap reflectors of Unit F to Unit E suggesting that forearc basin sediments were folded afterward, indicates continuous compression in the forearc basin.

[35] The boundary between the higher-angle backthrusts and the imbricated backthrusts is the base of Unit B, where the higher-angle backthrusts developed within the Middle Miocene–Upper Miocene forearc basin sediments deposited over the top of the accretionary (Figure 5). However, some of the higher-angle backthrusts seem to continue to the imbricated backthrusts beneath the inner wedge. A difference between displacements along these backthrusts can be observed (Figure 12). Displacement of the reflectors of Units A and B due to the higher-angle backthrusts seems to be smaller than that of the imbricated backthrusts.

[36] Beneath AR2, a blind-thrust has deformed sediments up to Unit E. This fault developed as the frontal part of the higher-angle backthrusts or here referred to as the Frontal Backthrust (FBT) of *Singh et al.* [2010] (Figure 5). Onlap reflectors of Unit F to Unit E can be observed on the limbs of the anticline. These observations indicate deformation took place after deposition of Unit E or during the Pliocene, subsequent to the higher-angle backthrusts beneath AR1.

4.2. Thrusting in the Forearc High

[37] In the forearc high, there are two types of thrusts that can be observed; the seaward-vergent imbricated forearc high thrusts (FHT) that originated in the accretionary wedge and the FHT′ that induced folding of the piggyback basin sediments deposited in the forearc high (Figure 6). The thrusts of the FHT have developed as 6–8 closely spaced (3–13 km) thrusts (Figures 3 and 11). Unit B shows thinning to the margin of the piggyback depression (Figure 6). Onlap of reflectors of Unit B to the top of the underlying accretionary wedge sediments can be observed. This onlap indicates that the piggyback depression in the forearc high have formed prior to deposition of Unit B, or during the Early-Middle Miocene. We interpret that the development of FHT might have controlled the development of piggyback depressions. The thrusts of the FHT seem to have formed initially as overturned anticlines and squeezed synclines in the top of the accretionary wedge. These thrusts have deformed the sediments, which may be the cause of chaotic reflectors to non-reflective zone within the accretionary wedge sediments. Therefore, even though the upper part of the accretionary wedge sediments has the same origin as the overlying forearc basin sediments, they have different seismic characters. Similar pattern of the FHT can be observed to the southeast of Enggano and south of western Java [*Schlüter et al.*, 2002; *Susilohadi et al.*, 2005], and have been mapped from outcrop in the forearc islands [*Andi Mangga et al.*, 1994; *Budhitrisna and Andi Mangga*, 1990; *Amin et al.*, 1993; *Yulihanto and Wiyanto*, 1999]. These observations indicate that this deformation affected a large region in the forearc high along the south Sumatra forearc.

[38] Based on pattern of the growth strata, the FHT′ involved sediments up to Unit D, where reflectors Unit E onlapped the deformed Unit D (Figure 6). This onlap indicates that the thrusts have formed prior to deposition of Unit D2 or during the Late Miocene. The thrusts of the FHT′ are interpreted to have formed due to the subsequent contraction of the accretionary wedge and these faults deformed the forearc basin sediments deposited in the piggyback depression.

5. Discussion

5.1. The MFZ and the Accretionary Wedge

[39] Based on the direction of the structures and interpretation of their sequential development, the two opposing vergence structures of the imbricated backthrusts and the forearc high thrusts can be interpreted as formerly two reverse kink bands that bounded a box fold during the onset of accretionary wedge deformation. This mechanism has been observed in sandbox modeling of accretionary wedge development [*Storti et al.*, 2000; *McClay et al.*, 2004; *Hoth et al.*, 2007; *Hardy et al.*, 2009]. The increased contraction induced shear along the landward-side kink band limb and formed a landward-vergent backthrust in the inner part of the accretionary wedge. In the seaward-side kink band limb, thrusts of the FHT formed in the hanging wall. All of these features can explain shear along backthrusts contemporaneously with the thrusts of the FHT developed in the hanging wall of the backthrust [*McClay et al.*, 2004; *Hoth et al.*, 2007]. Further contraction initiated the imbricated backthrusts in the inner wedge. Back-rotation of the FHT seems to have induced the contraction of the piggyback basin in the accretionary wedge, and initiated the higher-angle forearc high thrusts. Buckle folding and thrusting of sediments in the area between imbricated backthrusts and the forearc high thrusts may indicate contraction during the contemporaneous activity of these two

opposite-vergent thrusts. We interpret that there is no evidence of strike-slip fault system during the development of imbricated backthrusts in the MFZ.

[40] We suggest that the imbricated backthrusts continued along a fault surface that dips westward at 5–8° beneath the accretionary wedge. The slope of the interpreted fault surface seems to increase beneath the forearc high (∼14.5°) and terminates on top of the oceanic crust at 17 km depth (Figure 7). *Kopp et al.* [2001] have suggested that the subducting slab lies deeper at 19 km beneath the forearc high. The interpreted abrupt change in dip may reflect the geometry of the continental margin. We suggest that the materials in the footwall of this proposed backthrust underwent little deformation compared to the lithologies in the hanging wall and thus stronger materials are present in the footwall. Therefore, we suggest that the footwall of our interpreted backthrust is the backstop for the developing accretionary wedge. We suggest that the backstop is composed of sediments older than the basal part of the present forearc basin, or the Middle Miocene sediments and basement rocks. In the inner forearc basin, sediments of the Late Eocene to Early Miocene age have been identified beneath Middle Miocene sediments [*Hall et al.*, 1993]. The basement rocks have not been reached by drilling. However, metasediments and volcanics of Late Jurassic – Early Cretaceous have been observed onshore Sumatra [*Barber and Crow*, 2005]. Refraction seismic data have shown that the basement is continental in nature along southern Sumatra [*Kopp et al.*, 2001]. *Kopp and Kukowski* [2003] have suggested similar geometry of the backstop beneath the Sumatran forearc basin. We suggest that the backthrust could have developed along this continental backstop in the Mentawai region. Backthrusting and seaward dipping backstops have been proposed in the active accretionary wedges of the eastern Sunda arc [*Silver and Reed*, 1988], the Mediterranean ridge [*Le Pichon et al.*, 1982], and Lesser Antilles [*Westbrook et al.*, 1988; *Biju-Duval et al.*, 1982; *Byrne et al.*, 1993].

[41] The accretionary wedge attains a thickness of ∼7 km at the western margin of the present forearc basin and reaches ∼17 km thick beneath the forearc high (Figure 7). We suggest that the upper part of the accretionary wedge comprises materials from the arc side, as indicated by outcrops of the Upper Oligocene sediments in Siberut Island and blocks of the Eocene Nummulites limestones in Pagai and Sipora islands [*Yulihanto and Wiyanto*, 1999]. The thickness of the Middle Oligocene – Upper Miocene sediments observed in Nias Island was ∼6 km [*Samuel et al.*, 1997]. We suggest that the thickness of the accretionary wedge has been enhanced by the imbricated forearc high thrusts and imbricated backthrusts. Low velocities, which are indicative of sediments, have been observed beneath the forearc high that could be part of a paleo-accretionary wedge [*Kopp et al.*, 2001]. These low velocity zones have been interpreted as fluid-saturated overpressured sediments, as indicated by the high ratio of Vp/Vs [*Collings et al.*, 2012].

[42] Further contraction in the forearc took place after deposition of the forearc basin sediments in the accretionary wedge and forearc basin sediments. We suggest that this contraction formed the higher-angle backthrusts and induced folding of AR1. Intense deformation with backthrusts in the cores of the anticlines seems to induce reduction of the seismic velocities and loss of reflector continuity. We suggest that the continuous contraction of the forearc induced the FBT toward NE and folding of AR2. These observations indicate development of forward breaking fold-thrusts toward NE.

[43] Normal faults can be observed on the axis of anticlines, exhibiting collapse structures (Figure 12). We interpret this 2-km-wide feature to be related to subsurface volume loss due to mud migration and fluid escape within the underlying sediments. These collapsed structures, which are commonly associated with mud diapirism, developed by expulsion of materials from deeper along the faults [*Dimitrov*, 2002; *Singh et al.*, 2011]. The higher-angle backthrust may have formed a conduit for the materials injected upward. A conical feature on the seafloor is interpreted to be a mud volcano within the fold-thrust belt (Figures 10a and 13). We suggest that the development of diapirs and mud volcanoes is associated with the contemporaneous contraction that induced thrusting in the forearc basin sediments. Mud diapirism might be the cause of the poor reflectivity observed in these structures. Bottom-simulating reflectors (BSR) were imaged crossing the anticlines on all profiles indicating the base of the gas hydrate stability zone [*Kopp and Kukowski*, 2003].

[44] The features observed on the seismic profiles in the Mentawai forearc resemble diapirs and mud volcanoes reported in the offshore Madura basin [*Satyana and Asnidar*, 2008] and East Venezuela basin [*Duerto and McClay*, 2010]. Two active mud volcanoes have been identified within the MFZ in Nias Island [*Samuel and Harbury*, 1996]. Mud-related tectonism was also reported in the eastern Sunda subduction zone [*Barber et al.*, 1986; *Silver and Reed*, 1988]. It has been suggested that diapirs

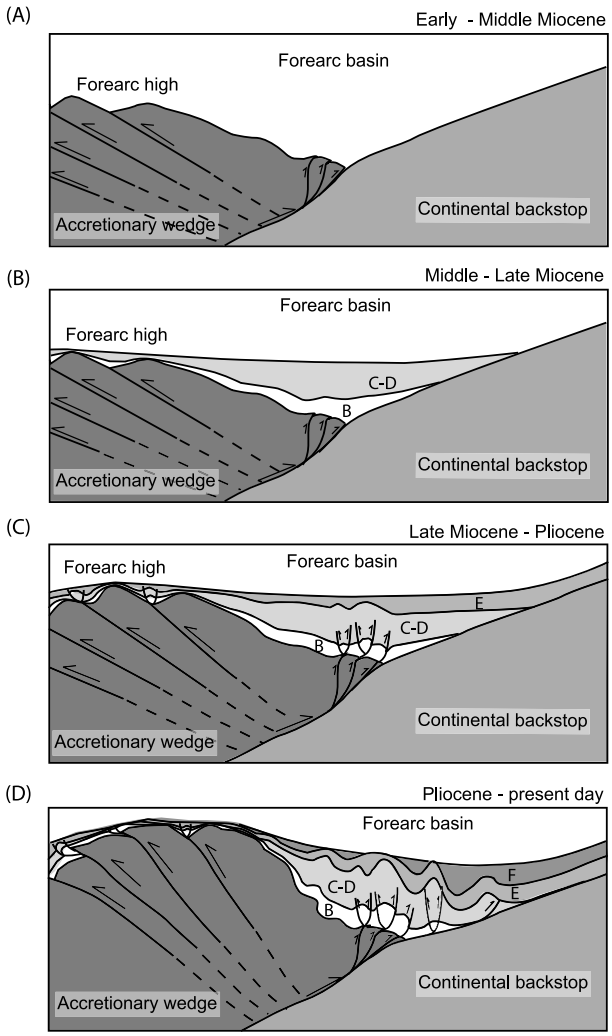

Figure 16. Schematic development stages of the MFZ.

and mud volcanoes were related to the activity along thrust faults [*Silver and Reed*, 1988; *Kopf*, 2002; *Duerto and McClay*, 2010].

[45] Changes of the dip of the thrusts can be observed between the imbricated backthrusts and the higher-angle backthrusts. The greater dips of the higher-angle backthrusts can be due to accommodation of some portion of the arc-parallel shear by these faults in such oblique convergence margin. However, the presence of mud-diapirs may give impression that the anticlinal ridges formed due to strike-slip motion. We did not find any en-echelon structures along the MFZ. The arcuate ridges are dominant structures observed on the seafloor indicating that these structures are associated with the compression of the accretionary wedge and forearc basin sediments. Furthermore, the younger splays of this developing fault system have developed in break-forward sequence, which is commonly observed in fold and thrust belts [e.g., *Shaw et al.*, 1999].

[46] The horsts and grabens can be observed which resemble the structures of the Paleogene basin (Figure 15) along the western Sumatran margin [*Barber and Crow*, 2005]. The higher-angle backthrusts may have correlated with the reactivation of these old structures as has been suggested by *Samuel and Harbury* [1996]. However, AR1 formed on top of a 3-km-wide horst structure, while AR2 developed above a graben structure. Therefore, there is no direct relation between these old extensional structures and backthrusts in the MFZ since the latter developed above different type of older structure. Furthermore, the Paleogene grabens developed as N-S and NE-SW trending structures in the northern and southern part of the Mentawai forearc basin, respectively [*Yulihanto and Wiyanto*, 1999; *Hall et al.*, 1993], whereas the younger structures are oriented NW-SE.

5.2. Structural Evolution of the Southern Sumatra Forearc

[47] The MFZ is likely to have initiated after the renewed subduction associated with development of the forearc high. However, the proposed timing of the renewed subduction varies from the Late Cretaceous [*Barber and Crow*, 2005], Paleocene [*Bellon et al.*, 2004], Mid-Eocene [*Hall et al.*, 2009] through to the Late Oligocene [*Karig et al.*, 1979]. Deposition of bathyal sediments took place on the slope of the forearc basin during the Middle Oligocene–Early Miocene [*Samuel et al.*, 1997]. This deposition indicates that a forearc high had not formed as a significant structural high compared to the present condition. After the incorporation of the arc-derived materials into the slope basin, the forearc high thrusts are developed as seaward-vergent imbricated thrusts, and resulting in the formation of a forearc high during the latest Early Miocene. The imbrication of the forearc high thrusts might have contributed to the intense deformation of sediments beneath the top of the accretionary wedge. At the same time, the imbricated backthrusts had formed at the toe of the inner part of the accretionary wedge (Figure 16a). The development of forearc high thrusts and imbricated backthrusts induced the uplift of the forearc high as indicated by thinning of the Middle Miocene sediments to the forearc high. The rise of the forearc high may explain the unconformity between Middle Miocene sediments and the overlying formations in Siberut and Nias islands that have been observed by *Samuel et al.* [1997] and *Andi Mangga et al.* [1994]. The initiation of the imbricated backthrusts and the

forearc high thrusts precedes the inception of Sumatra Fault, which *McCarthy and Elders* [1997] have suggested to have occurred in Middle Miocene.

[48] The Middle to Late Miocene was the period of deposition of thick transgressive-regressive sediments in the forearc basin related to uplift in the core of Sumatra. The activity of imbricated backthrusts waned as indicated by no significance deformation in the growth strata (Figure 16b). The area where these backthrusts was initiated became the depocenters of the forearc basin, expressed by the maximum thickness of the sediments. To the west, the coeval sediments show thinning to the uplifted forearc high.

[49] During the Late Miocene, the higher angle backthrusts were initiated and deformed the forearc basin sediments (Figure 16c). Mud diapirism was active since the Early Pliocene. The deformation might have been induced by further contraction of the accretionary wedge and forearc basin sediments. The initiation of the higher angle backthrusts coincides with the interpreted offscraping of thick Bengal Fan sediments during the Late Miocene [*Karig et al.*, 1979; *Beaudry and Moore*, 1981], which might have induced thickening of the frontal accretionary wedge. The thickening of the frontal-wedge can be associated with an increase of compressional stresses along its base [*van der Werff*, 1996, *Karig et al.*, 1979; *Kopp and Kukowski*, 2003]. An increase in plate convergence has also been suggested during the Late Miocene [*Karig et al.*, 1979; *Lee and Lawver*, 1995].

[50] The continuous contraction of the forearc led to the progressive deformation in the forearc basin toward Sumatra (Figure 16d). Since the Pliocene, fold-thrust belt developed above the detachment fault. The shale tectonics-induced fold-thrust is evidenced by the formation of diapirs and mud volcanoes. Diapirs and mud volcanoes explained the presence of mélange in Nias and Mentawai islands that contained a matrix of Oligo-Miocene sediments and older ophiolitic inclusions [*Samuel et al.*, 1997; *Andi Mangga et al.*, 1994; *Budhitrisna and Andi Mangga*, 1990]. The continuous contraction of the forearc induced the Pliocene uplift in the forearc high and western part of the forearc basin.

5.3. Earthquake and Tsunami Risks Due to Backthrust

[51] Based on high reflectivity of the deep-rooted backthrusts in 2004 and 2007 earthquake rupture zones, *Singh et al.* [2011] suggested that these backthrusts might have ruptured co-seismically enhancing the reflectivity due to fluid flow from the mantle. Headwall scarps of past landslides can be observed on the limb of the anticlines. *Singh et al.* [2010] suggested that mass wasting occurred in the vicinity of the MFZ at the NE margin of Siberut-Pagai islands. Landslide of large portion of the anticlinal ridges in the future could generate a large tsunami in the Mentawai basin area.

[52] Relocated seismicity using the double difference method [*Pesicek et al.*, 2010] is shown in Figure 17. Within the MFZ, two clusters of seismicity can be observed near Siberut–Sipora and Enggano islands, with several thrust earthquakes. Alignment of seismic events down to 30 km depth can be observed along the forearc high indicating that compression dominated the slip. However, there is a lack of shallow seismicity along the MFZ (Figure S4a). There is only one event observed along the MFZ at ~10 km depth with no information on the focal mechanism. Slip along a possible backthrust within the forearc is suggested by a cluster of seismicity located in the Mentawai area west of Pagai, some with thrust focal mechanism [*Collings et al.*, 2012], and to the south of Siberut [*Wiseman et al.*, 2011]. A lack of shallow seismicity also can be observed in the forearc high (Figure S4). However, tilting of the forearc high toward NE to the north of Enggano Island may indicate the activity of the FHT (Figure 9). We suggest that the activity of backthrusts is waning, as indicated by the decrease in deformation within the sequential development of the backthrusts. The frontal higher-angle backthrusts in the MFZ have developed as blind thrusts that only folded the thick overlying sediments. The accumulated slip within the latest episode of backthrusting seems to be small. However, the size of the backthrust fault plane is large enough to produce large magnitude event. Since the backthrusts are waning in activity, the possibility of seismic hazard along the backthrusts at the present time should be small.

6. Conclusions

[53] The MFZ, which previously has been considered as a strike-slip fault zone is interpreted to have formed as a backthrust and fold-thrust belt in the deeper forearc basin. On the seafloor, deformation of the MFZ is marked by arcuate anticlinal ridges, convex toward NE, along the western margin of the present Mentawai forearc basin. Beneath the anticlinal ridges the deformation zone exhibits (1) landward-vergent imbricated backthrusts in the inner part of the accretionary wedge, and (2) landward-vergent higher-angle

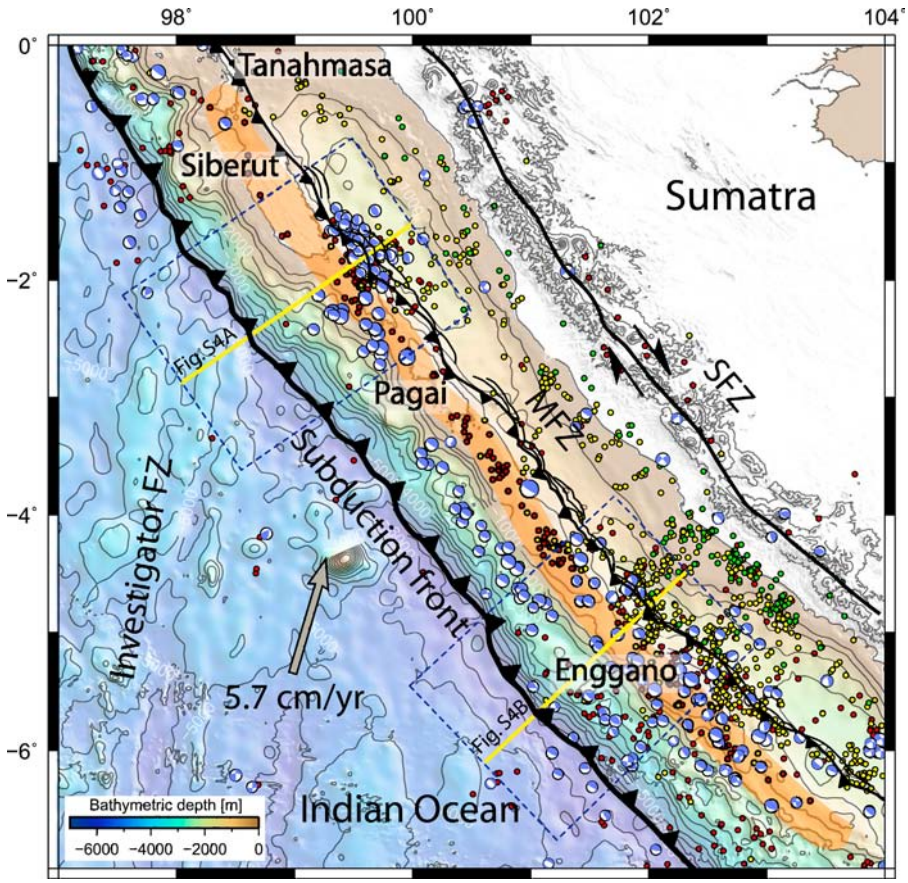

Figure 17. Map of the MFZ along the basin. Black solid line represents the projection of MBT. Thin black lines represent axis of folds formed in the fold-thrust belt. Shaded orange represents the FHT distribution. Red, yellow and green circles represent relocated earthquakes with depth of 0–30, 30–60, and 60–90 km, respectively [*Pesicek et al.*, 2010]. Beach balls represent the GCMT focal mechanisms plotted at their centroid locations (1976–2010) for earthquake ∼30 km depth. Yellow lines marked the profile shown in Figure S4. Dashed rectangles show the swath of the projection of hypocenters and focal mechanisms.

backthrusts that deformed the forearc basin sediments. In the forearc high, anticlinal ridges formed due to the seaward-vergent forearc high thrusts originating in the accretionary wedge. We interpret that backthrusting was initiated during the Early-Middle Miocene with the slide and back-rotation of the forearc high thrusts. In the Late Miocene, the higher-angle backthrusts was initiated, increasing the uplift of the anticlines. The continuous contraction initiated the frontal higher-angle backthrusts that formed a fold-thrust belt toward the east during the Pliocene. The folds and thrusts were disturbed by diapirs and mud volcanoes. The backthrusts show waning in activity and hence the risk of a large earthquake and associated tsunami at the present time should be small.

Acknowledgments

[54] The authors thank TGS and CGGVeritas for permission to use their data. We acknowledge Manuel Pubellier, Nathalie Feuillet, Cipi Armandita and Hade Maulin for the discussions. Pascal Richet read original version of the manuscript and provided comments and suggestions. Critical reviews and constructive suggestions from Robert Hall, two anonymous reviewers and the editor (Thorsten Becker) improved the clarity of the manuscript. This is IPGP contribution 3349.

References

Amin, T. C., E. Kusnama Rustandi, and S. Gafoer (1993), Geological map of the Manna and Enggano sheet, Sumatera, scale 1: 250.000, Geol. Res. and Dev. Cent., Bandung, Indonesia.

Andi Mangga, S., G. Burhan Sukardi, and E. Suryanila (1994), Geological map of the Siberut sheet, Sumatera, scale 1: 250.000, Geol. Res. and Dev. Cent., Bandung, Indonesia.

Barber, A. J., and M. J. Crow (2005), Structure and structural history, in *Sumatra Geology, Resources and Tectonic Evolution*, edited by A. J. Barber, M. J. Crow, and J. S. Milsom, *Geol. Soc. Lond. Mem.*, *31*, 175–233.

Barber, A. J., S. Tjokrosapoetro, and T. R. Charlton (1986), Mud volcanoes, shale diapirs, wrench faults and Melanges in accretionary complex, *AAPG Bull.*, *70*, 1729–1741.

Beaudry, D., and G. F. Moore (1981), Seismic-stratigraphic framework of the forearc basin off Central Sumatra, Sunda Arc, *Earth Planet. Sci. Lett.*, *54*, 17–28, doi:10.1016/0012-821X(81)90065-0.

Bellon, H., R. C. Maury, Sutanto, R. Soeria-Atmadja, J. Cotton, and M. Polve (2004), 65 m.y.-long magmatic activity in Sumatra (Indonesia), from Paleocene to Present, *Bull. Soc. Geol. Fr.*, *175*, 61–72.

Berglar, K., C. Gaedicke, D. Franke, S. Ladage, F. Klingelhoefer, and Y. S. Djajadiharddja (2010), Structural evolution and strike-slip tectonics off north-western Sumatra, *Tectonophysics*, *480*, 119–132.

Biju-Duval, B., B. P. Le Quellec, A. Mascle, V. Renard, and P. Valey (1982), Multibeam bathymetric survey and high resolution seismic investigations on the Barbados ridge complex (eastern Caribbean): A key to the knowledge and interpretation of an accretionary wedge, *Tectonophysics*, *86*, 275–304, doi:10.1016/0040-1951(82)90070-1.

British Oceanographic Data Centre (2003), *GEBCO Digital Atlas: Centenary Edition of the IOC/IHO General Bathymetric Chart of the Oceans* [CD-ROM], Liverpool, U. K.

Budhitrisna, T., and S. Andi Mangga (1990), Geological map of the Pagai and Sipora quadrangle, Sumatra, scale 1: 250.000, Geol. Res. and Dev. Cent., Bandung, Indonesia.

Byrne, D., W. Wang, and D. M. Davis (1993), Mechanical role of backstops in the growth of forearcs, *Tectonics*, *12*, 123–144, doi:10.1029/92TC00618.

Chlieh, M., J.-P. Avouac, K. Sieh, D. H. Natawidjaja, and J. Galetzka (2008), Heterogeneous coupling of the Sumatran megathrust constrained by geodetic and paleogeodetic measurements, *J. Geophys. Res.*, *113*, B05305, doi:10.1029/2007JB004981.

Collings, R., D. Lange, A. Rietbrock, F. Tilmann, D. Natawidjaja, B. Suwargadi, M. Miller, and J. Saul (2012), Structure and seismogenic properties of the Mentawai segment of the Sumatra subduction zone revealed by local earthquake traveltime tomography, *J. Geophys. Res.*, *117*, B01312, doi:10.1029/2011JB008469.

Diament, M., H. Harjono, K. Karta, C. Deplus, D. Dahrin, M. T. Zen, M. Gerard, O. Lassal, A. Martin, and J. Malod (1992), Mentawai fault zone off Sumatra: A new key to the geodynamics of western Indonesia, *Geology*, *20*, 259–262, doi:10.1130/0091-7613(1992)020<0259:MFZOSA>2.3.CO;2.

Dimitrov, L. I. (2002), Mud volcanoes—The most important pathway for degassing deeply buried sediments, *Earth Sci. Rev.*, *59*, 49–76, doi:10.1016/S0012-8252(02)00069-7.

Duerto, L., and K. McClay (2010), Role of the shale tectonics on the evolution of the Eastern Venezuelan Cenozoic thrust and fold belt, *Mar. Pet. Geol.*, *28*, 81–108, doi:10.1016/j.marpetgeo.2009.11.005.

Hall, D. M., B. A. Duff, M. C. Courbe, B. W. Seubert, M. Siahaan, and A. D. Wirabudi (1993), The southern fore-arc zone of Sumatra: Cainozoic basin-forming tectonism and hydrocarbon potential, paper presented at 22nd IPA Annual Convention and Exhibition, Indonesian Pet. Assoc., Jakarta.

Hall, R., B. Clements, and H. Smyth (2009), Sundaland: Basement Character, Structure and Plate Tectonic Development, paper presented at 33rd IPA Annual Convention and Exhibition, Indonesian Pet. Assoc., Jakarta.

Hardy, S., K. McClay, and J. A. Muñoz (2009), Deformation and fault activity in space and time in high-resolution numerical models of doubly vergent thrust wedges, *Mar. Pet. Geol.*, *26*, 232–248, doi:10.1016/j.marpetgeo.2007.12.003.

Hoth, S., A. Hoffmann-Rothe, and N. Kukowski (2007), Frontal accretion: An internal clock for bivergent wedge deformation and surface uplift, *J. Geophys. Res.*, *112*, B06408, doi:10.1029/2006JB004357.

Karig, D. E., S. Suparka, G. F. Moore, and P. E. Hehanussa (1979), Structure and Cenozoic evolution of the Sunda Forearc in the Central Sumatra region, in *Geological and Geophysical Investigation of Continental Margin*, edited by J. S. Watkins, L. Montadert, and P. Wood-Dickerson, *AAPG Memoir*, *29*, 223–237.

Kopf, A. J. (2002), Significance of mud volcanism, *Rev. Geophys.*, *40*(2), 1005, doi:10.1029/2000RG000093.

Kopp, H., and N. Kukowski (2003), Backstop geometry and accretionary mechanics of the Sunda margin, *Tectonics*, *22*(6), 1072, doi:10.1029/2002TC001420.

Kopp, H., E. R. Flueh, D. Klaeschen, J. Bialas, and C. Reichert (2001), Crustal structure of the central Sunda margin at the onset of oblique subduction, *Geophys. J. Int.*, *147*(2), 449–474, doi:10.1046/j.0956-540x.2001.01547.x.

Ladage, S., W. Weinrebe, C. Gaedicke, U. Barckhausen, E. R. Flueh, I. Heyde, A. Krabbenhoeft, H. Kopp, S. Fajar, and Y. S. Djajadihardja (2006), Bathymetric survey images structure off Sumatra, *Eos Trans. AGU*, *87*(17), 165–172, doi:10.1029/2006EO170001.

Lee, T. T., and L. A. Lawver (1995), Cenozoic plate reconstruction of Southeast Asia, *Tectonophysics*, *251*, 85–138, doi:10.1016/0040-1951(95)00023-2.

Le Pichon, X., N. Lybéris, J. Angelier, and V. Renard (1982), Strain distribution over the Mediterranean Ridge: A synthesis incorporating new Sea-Beam data, *Tectonophysics*, *86*, 243–274, doi:10.1016/0040-1951(82)90069-5.

Malod, J. A., and B. M. Kemal (1996), The Sumatra margin: Oblique subduction and lateral displacement of the accretionary prism, in *Tectonic Evolution of Southeast Asia*, edited by R. Hall and D. Blundell, *Geol. Soc. Spec. Publ.*, *106*, 19–28, doi:10.1144/GSL.SP.1996.106.01.03.

McCaffrey, R., P. Zwick, Y. Bock, L. Prawirodirdjo, J. Genrich, C. W. Stevens, S. S. O. Puntodewo, and C. Subarya (2000), Strain partitioning during oblique plate convergence in northern Sumatra: Geodetic and seismologic constraints and numerical modeling, *J. Geophys. Res.*, *105*, 28,363–28,376, doi:10.1029/1999JB900362.

McCarthy, A. J., and C. F. Elders (1997), Cenozoic deformation in Sumatra: Oblique subduction and the development of the Sumatran Fault, in *Petroleum Geology of Southeast Asia*, edited by A. J. Fraser and S. J. Matthews, *Geol. Soc. Spec. Publ.*, *126*, 355–363, doi:10.1144/GSL.SP.1997.126.01.21.

McClay, K. R., P. S. Whitehouse, T. Dooley, and M. Richards (2004), 3D evolution of fold and thrust belts formed by oblique convergence, *Mar. Pet. Geol.*, *21*, 857–877, doi:10.1016/j.marpetgeo.2004.03.009.

Milsom, J. S. (2005), Seismology and neotectonics, in *Sumatra Geology, Resources and Tectonic Evolution*, edited by A. J. Barber, M. J. Crow, and J. S. Milsom, *Geol. Soc. Mem.*, *31*, 8–15.

Mosher, D., J. Austin Jr., D. Fisher, and S. Gulick (2008), Deformation of the northern Sumatra accretionary prism from high-resolution seismic reflection profiles and ROV observations, *Mar. Geol.*, *252*(3–4), 89–99.

Natawidjaja, D. H., K. Sieh, J. Galetzka, B. W. Suwargadi, H. Cheng, and R. L. Edwards (2006), Source Parameters of the great Sumatran megathrust earthquakes of 1797 and 1833 inferred from coral microatolls, *J. Geophys. Res.*, *111*, B06403, doi:10.1029/2005JB004025.

Pesicek, J. D., C. H. Thurber, H. Zhang, H. R. DeShon, E. R. Engdahl, and S. Widiyantoro (2010), Teleseismic double-difference relocation along the Sumatra-Andaman subduction

zone using a 3-D model, *J. Geophys. Res.*, *115*, B10303, doi:10.1029/2010JB007443.

Poblet, J., K. McClay, F. Storti, and J. A. Munoz (1997), Geometries of syntectonic sediments associated with single-layer detachment folds, *J. Struct. Geol.*, *19*(3–4), 369–381, doi:10.1016/S0191-8141(96)00113-7.

Prawirodirdjo, L., and Y. Bock (2004), Instantaneous global plate motion model from 12 years of continuous GPS observations, *J. Geophys. Res.*, *109*, B08405, doi:10.1029/2003JB002944.

Samuel, M. A., and N. A. Harbury (1996),The Mentawai fault zone and deformation of the Sumatran forearc in the Nias area, in *Tectonic Evolution of SE Asia*, edited by R. Hall and D. J. Blundell, *Geol. Soc. Spec. Publ.*, *106*, 337–351, doi:10.1144/GSL.SP.1996.106.01.22.

Samuel, M. A., N. A. Harbury, A. Bakri, F. Banner, and L. Hartono (1997), A new stratigraphy for the islands of the Sumatran Forearc, Indonesia, *J. Asian Earth Sci.*, *15*, 339–380, doi:10.1016/S0743-9547(97)87720-3.

Satyana, A. H., and Asnidar (2008), Mud diapirs and mud volcanoes in depressions of Java to Madura: Origins, natures, and implications to petroleum system, paper presented at 32nd IPA Annual Convention, Indonesian Pet. Assoc., Jakarta.

Schlüter, H. U., C. Gaedicek, H. A. Roeser, B. Schreckenberger, H. Meyer, C. Reichert, Y. Djajadiharja, and A. Prexl (2002), Tectonic features of the southern Sumatra-western Java forearc of Indonesia, *Tectonics*, *21*(5), 1047, doi:10.1029/2001TC901048.

Shaw, J. H., F. Bilotti, and P. A. Brennan (1999), Patterns of imbricate thrusting, *Geol. Soc. Am. Bull.*, *111*(8), 1140–1154, doi:10.1130/0016-7606(1999)111<1140:POIT>2.3.CO;2.

Silver, E. A., and D. L. Reed (1988), Backthrusting in accretionary wedges, *J. Geophys. Res.*, *93*, 3116–3126, doi:10.1029/JB093iB04p03116.

Singh, S. C., R. W. Hobbs, and D. B. Snyder (1996), Broadband receiver response from dual-streamer data and applications in deep reflection seismology, *Geophysics*, *61*, 232–243, doi:10.1190/1.1443944.

Singh, S. C., S. Midnet, and Y. S. Djajadihardja (2009), Seismic survey of the locked and unlocked Sumatra subduction zone, *Eos Trans. AGU*, *90*(49), 471–478, doi:10.1029/2009EO490002.

Singh, S. C., N. D. Hananto, A. P. S. Chauhan, H. Permana, M. Denolle, A. Hendriyana, and D. Natawidjaja (2010), Evidence of active backthrusting at the NE margin of Mentawai Islands, SW Sumatra, *Geophys. J. Int.*, *180*, 703–714, doi:10.1111/j.1365-246X.2009.04458.x.

Singh, S. C., N. D. Hananto, and A. P. S. Chauhan (2011), Enhanced reflectivity of backthrusts in the recent great Sumatran earthquake rupture zones, *Geophys. Res. Lett.*, *38*, L04302, doi:10.1029/2010GL046227.

Storti, F., F. Salvini, and K. R. McClay (2000), Velocity-partitioned synchronous thrusting and thrust polarity reversal in experimental doubly vergence thrust wedges accreted at different syntectonic sedimentation rates: Implications for natural orogens, *Tectonics*, *19*, 378–396, doi:10.1029/1998TC001079.

Susilohadi, S., C. Gaedicke, and A. Ehrhardt (2005), Neogene structures and sedimentation history along the Sunda forearc basins off southwest Sumatra and southwest Java, *Mar. Geol.*, *219*, 133–154, doi:10.1016/j.margeo.2005.05.001.

van der Werff, W. (1996), Variation in forearc basin development along the Sunda Arc, Indonesia, *J. Southeast Asian Earth Sci.*, *14*, 331–349, doi:10.1016/S0743-9547(96)00068-2.

Wang, K., and Y. Hu (2006), Accretionary prisms in subduction earthquake cycles: The theory of dynamic Coulomb wedge, *J. Geophys. Res.*, *111*, B06410, doi:10.1029/2005JB004094.

Wessel, P., and W. Smith (1991), Free software helps map and display data, *Eos Trans. AGU*, *72*(41), 441, doi:10.1029/90EO00319.

Westbrook, G. K., J. W. Ladd, P. Buhl, N. Bangs, and G. J. Tiley (1988), Cross section of an accretionary wedge: Barbados Ridge complex, *Geology*, *16*, 631–635, doi:10.1130/0091-7613(1988)016<0631:CSOAAW>2.3.CO;2.

Wiseman, K., P. Banerjee, K. Sieh, R. Bürgmann, and D. Natawidjaja (2011), Another potential source of destructive earthquakes and tsunami offshore of Sumatra, *Geophys. Res. Lett.*, *38*, L10311, doi:10.1029/2011GL047226.

Yulihanto, B., and B. Wiyanto (1999), Hydrocarbon potential of the Mentawai forearc basin West Sumatra, paper presented at 27th IPA Annual Convention and Exhibition, Indonesian Pet. Assoc., Jakarta.

Structural evolution of backthrusting in the Mentawai Fault Zone, offshore Sumatran forearc

Supplementary materials

Figure S1. (A) Uninterpreted seismic section, (B) Interpreted seismic section of line SSS-133 across the MFZ. Note the step-like pattern above the MBT and FBT.

Figure S2. (A) Uninterpreted seismic section, (B) Interpreted seismic section of line SMI-219 across the MFZ. Collapsed structure formed a depression at the top of Unit D above the anticline.

Figure S3. (A) Uninterpreted seismic section, (B) Interpreted seismic section of line 13 across the MFZ.

Figure S4. Projection of hypocenters and focal mechanisms along lines crossing the northwestern (A) and southeastern part (B) of Mentawai forearc. Thrust events occurred in the area of the backthrust and fold-thrust belt.

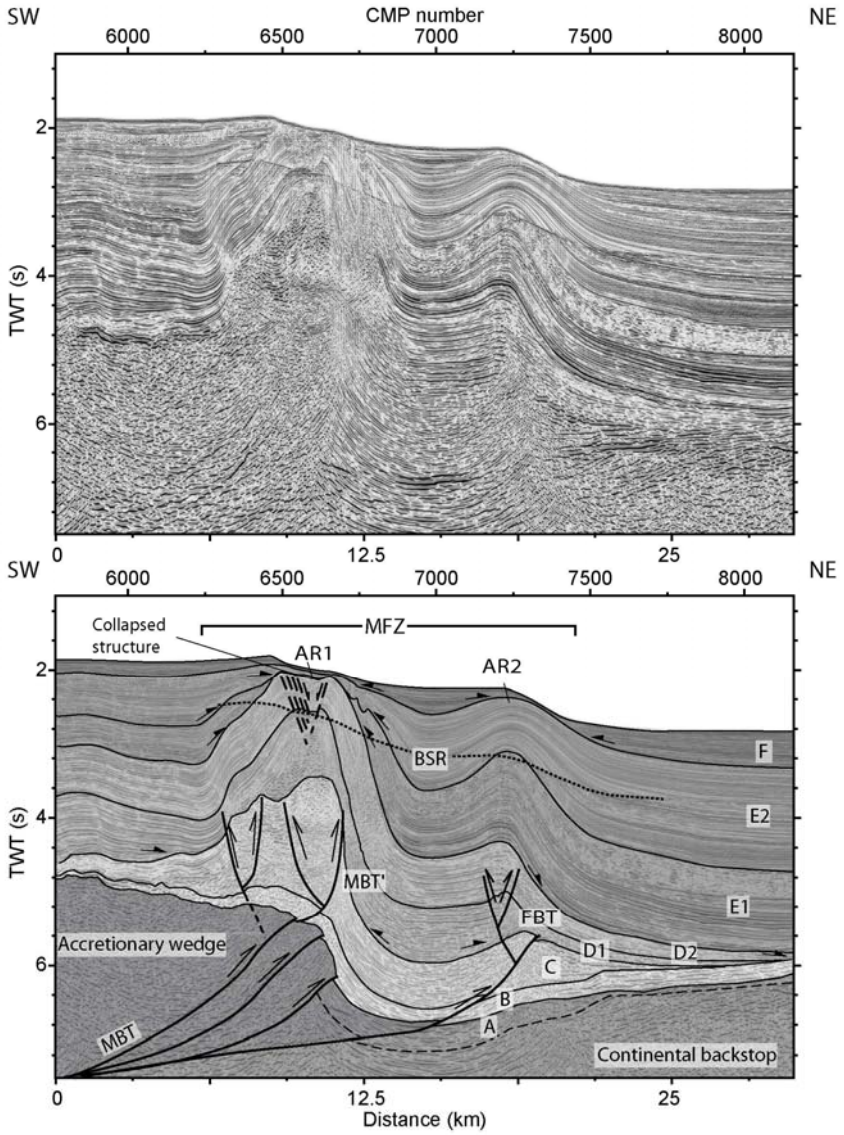

Figure S1. (A) Uninterpreted seismic section, (B) Interpreted seismic section of line SSS-133 across the MFZ. Note the step-like pattern above the MBT and FBT.

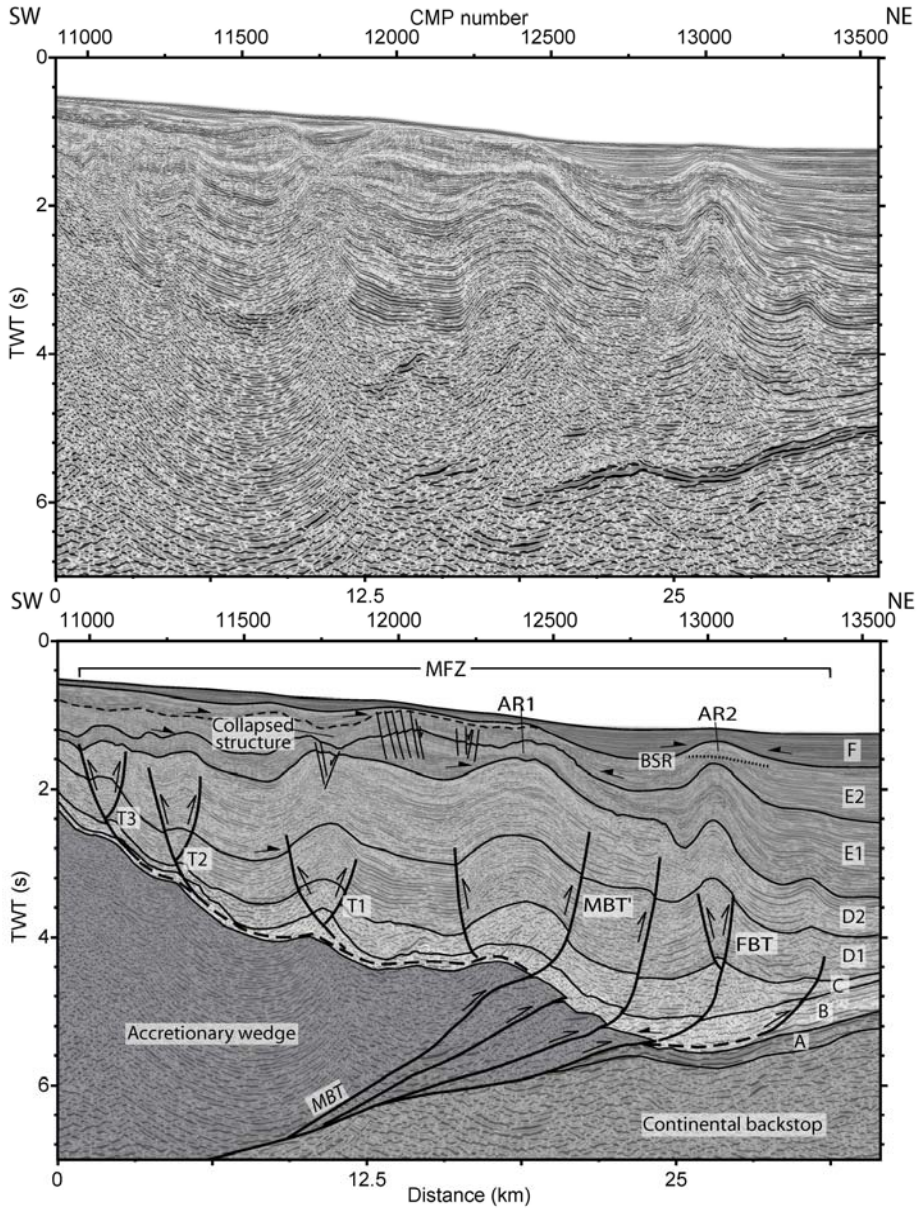

Figure S2. (A) Uninterpreted seismic section, (B) Interpreted seismic section of line SMI-219 across the MFZ. Collapsed structure formed a depression at the top of Unit D above the anticline.

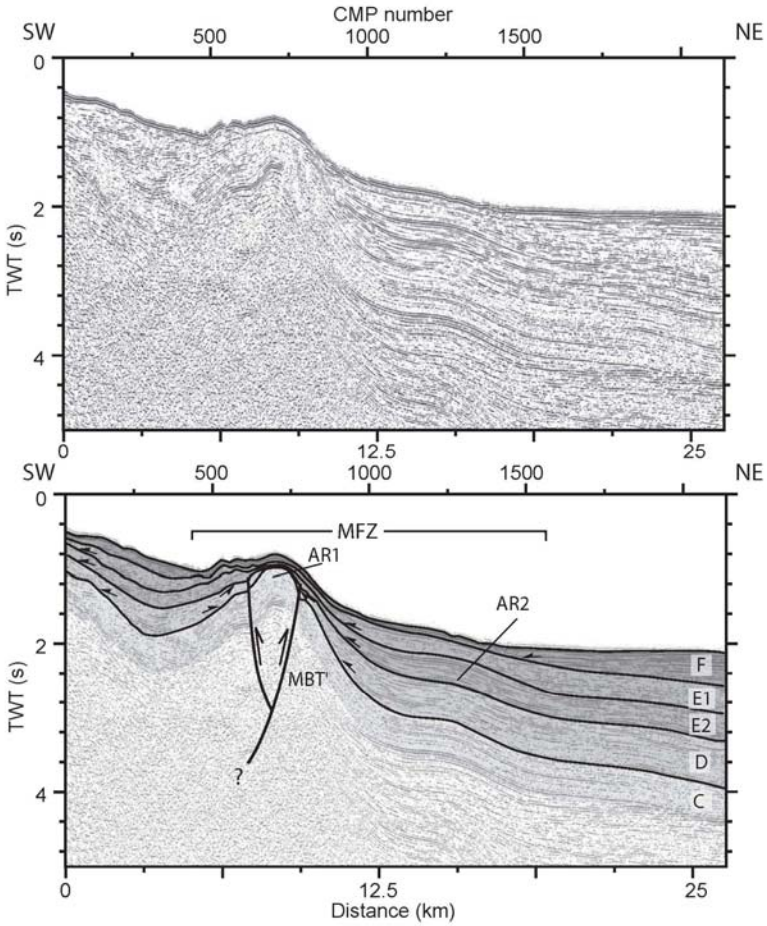

Figure S3. (A) Uninterpreted seismic section, (B) Interpreted seismic section of line 13 across the MFZ

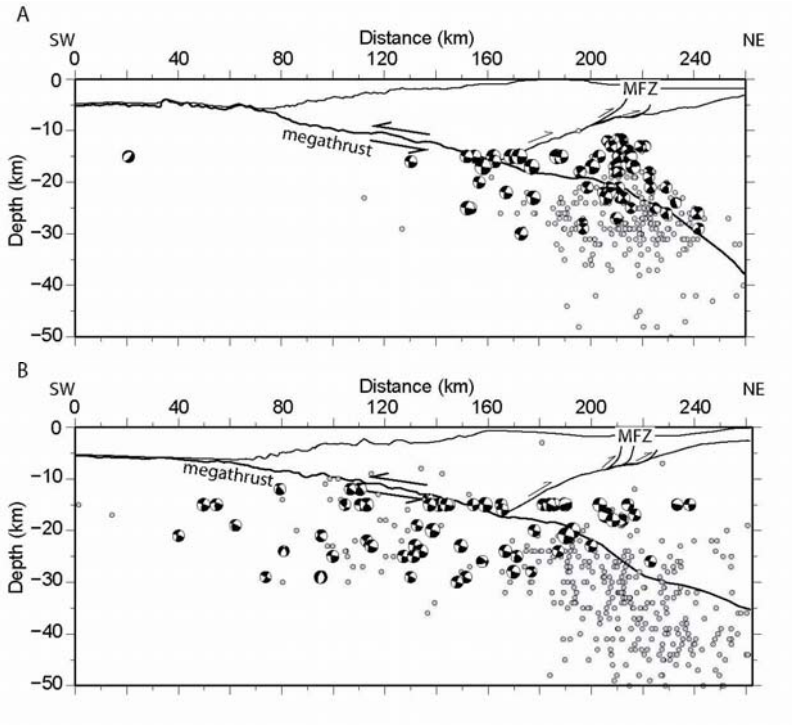

Figure S4. Projection of hypocenters and focal mechanisms along lines crossing the northwestern (A) and southeastern part (B) of Mentawai forearc. Thrust events occurred in the area of the backthrust and fold-thrust belt.